THE INTERACTION OF ELECTROMAGNETIC WAVES WITH VO_2 NANOSIZED SPHERES AND FILMS IN OPTICAL AND EXTREMELY HIGH FREQUENCY RANGE

V.V. Koledov[1], V.G. Shavrov[1], N.V. Shahmirzadi[2], T. Pakizeh[2], A.P. Kamantsev[1], D.S. Kalenov[1], M.P. Parkhomenko[1], S.V. von Gratowski[1], A.V. Irzhak[3,4], V.M. Serdyuk[5], J.A. Titovitsky[5], A.A. Komlev[6], A.E. Komlev[6], D.A. Kuzmin[7], I.V. Bychkov[7]

[1]Kotelnikov Institute of Radioengineering and Electronics of Russian Academy of Sciences, Mokhovaya 11-7, Moscow 125009, Russia
[2]Faculty of Electrical Engineering, K.N. Toosi University of Technology, Tehran 19697, Iran
[3]National University of Science and Technology MISiS, Leninskii pr. 4, Moscow 119049, Russia
[4]Institute of Microelectronic Technology and High Purity Materials of Russian Academy of Sciences, Ac. Osipyana 6, Chernogolovka, Moscow Region 142432, Russia
[5]Institute of Applied Physical Problems, Belarusian State University, Kurchatova 7, Minsk 220045, Belarus
[6]Saint-Petersburg Electrotechnical University "LETI", Prof. Popova 5, St.-Petersburg 197376, Russia
[7]Chelyabinsk State University, Br. Kashirinykh 129, Chelyabinsk 454001, Russia

The paper is received on February 20, 2018

Abstract. Recently the interaction effects of electromagnetic waves (EMW) with metallic nanoparticles and holes in nanosized films, called nano-antennas (NAs) attract great interest because of prospective applications in sensors technology. The conventional NAs and nanoparticles have fixed functionality, therefore the tunability of these structures are desired. One of the conventional method to obtain tunability is exploiting phase transition (PT) materials. Vanadium dioxide (VO_2) is known as a PT material and its complex dielectric constant are varied by temperature due to structural transformation, accompanying metal-insulator transition (MIT). This material is an insulator at room temperature (RT) and becomes metal above a critical temperature (T_c=340 K). Hence, this material has emerged new applications in various fields. In this paper, VO_2 film on glass substrate were prepared and investigated in extremely high frequency (EHF) range (27–37 GHz). Then submicron holes arrays were formed on VO_2 films and their optical Raman spectra were studied. The special attention is paid on temperature dependence of the properties of films, holes and spheres. The study of EHF response of the nanosized VO_2 films reveals strong anomalies in the temperature range of metal-insulator transition. The

submicron holes and arrays show strong change of the Raman spectra at the wavelength 530 nm due to heating by laser beam. Eventually, the optical properties of the homogeneous nonmagnetic VO_2 nanospheres embedded in the air are studied theoretically. The size effects on the optical properties of the VO_2 nanosphere are investigated and presented. In VO_2 nanosphere, converting into the metallic phase by heating leads to formation of a localized surface plasmon resonance (LSPR) which red shifts slightly by increasing dimension. The increment in the dimension of nanosphere in insulator case, results in the appearance of a peak in the visible wavelength most probably due to the excitation of combined electromagnetic modes. The optical spectra of VO_2 nanoparticle are much broader than that of silver nanosphere, which its associated localized electric field in form of dipolar mode is more intense than in VO_2 case. However, the LSPR of VO_2 can be thermally switched, making this material peculiar for recent advanced applications.

Keywords: phase transition, VO_2, nano-antenna, nano-spheres, nano-holes, surface plasmon resonance, Raman spectrum, extremely high frequency, optical frequency.

1. Introduction

In the last decade a real breakthrough has been made in the field of nano-photonics, nano-plasmonics, NAs, and metasurfaces (optical nanomaterials). One of the main problems facing the wide application of these devices is that these properties of such devices are fixed at the time of manufacture during their creation, and they cannot be tuned. Controllable, or as they are called in these areas "active" (not to be confused with energy-generating) devices would not only be much more in demand, but could create many new scientific and technical opportunities for science and technology.

In this direction, great efforts are being made. So it should be noted the configurable antennas and metasurfaces [1], based on a change in carrier substrate density [2-5], active devices based on liquid crystals, functioning by changing the effective index of a liquid crystal by an electric and magnetic field [6, 7] and electrically controlled active devices [8-10]. According to many reports, materials

with phase transitions (PT), for example, metal-insulator transition (MIT), are the most promising materials for creating the devices described above with control properties. A review of the work in this area is given in [11]. The Figs. 1-3 clearly illustrates the functional properties of oxide materials with MIT, devices based on them and areas of their applications.

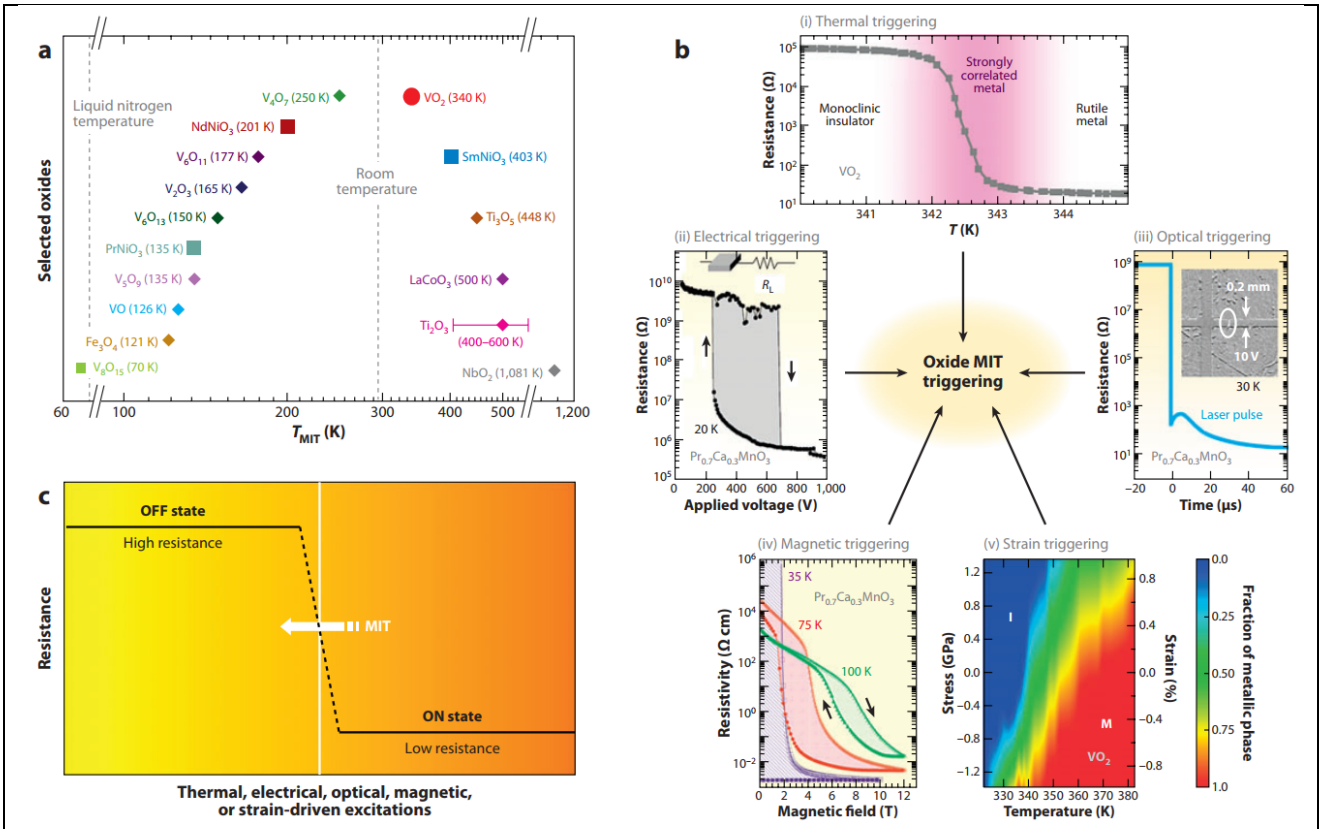

Fig. 1. The metal-insulator transition (MIT) switch. (*a*) MIT temperature (*T*MIT) of some selected oxides (bulk crystals). External stress or substrate-driven constraints can significantly influence the transition temperature and the resistivity change. (*b*) MIT-triggering approaches in correlated oxides. (*i*) Temperature-triggered MIT in VO_2. (*ii*) Electrically triggered MIT in $Pr_{0.7}Ca_{0.3}MnO_3$. (*iii*) Optically triggered MIT in $Pr_{0.7}Ca_{0.3}MnO_3$. (*iv*) Magnetically triggered MIT in $Pr_{0.7}Ca_{0.3}MnO_3$. (*v*) Strain/ stress effects on MIT in VO_2. (*c*) Basic concept of utilizing MIT in correlated oxides as a switch, with the high-resistance, insulating and low-resistance, metallic states on both sides of MIT, defined as OFF and ON states, respectively. The switching of the device can be triggered thermally, electrically, optically, magnetically, and by strain drive, corresponding to the MIT-triggering approaches shown in panel *b* [11].

Some of the most interesting materials with MIT are oxides of some d-elements, such as NiO, CoO, and VO_2. These materials have partially filled with electrons d-shells of atoms and, from the point of view of the band theory, are metals, however, they have a forbidden band (namely, the Mott-Hubbard gap) in the electronic spectrum, which changes its width under certain conditions, for example,

temperature, pressure, etc. In such materials, under the influence of external factors, MIT is observed.

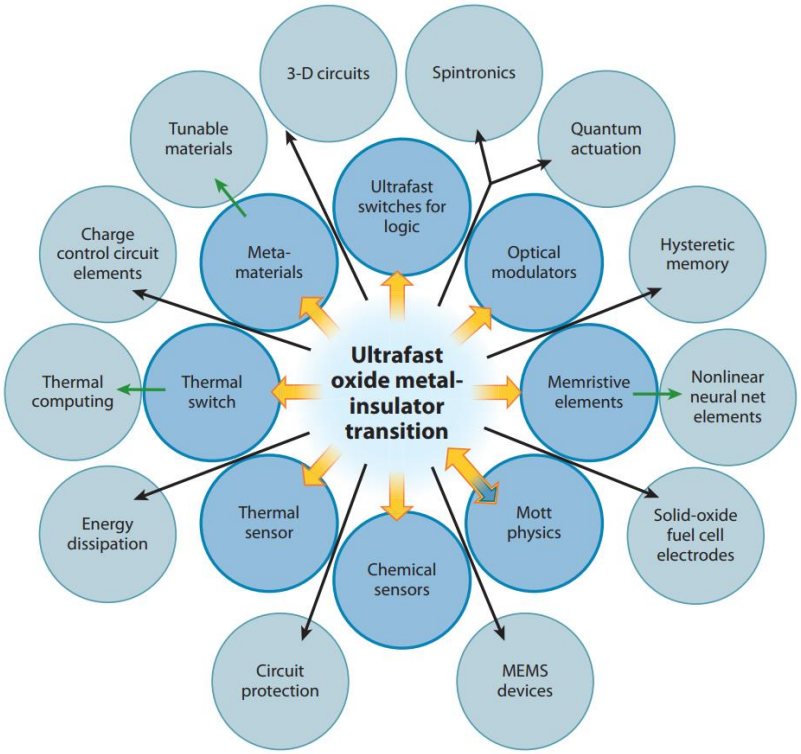

Fig. 2. Prospective applications of the functional materials with MIT [11].

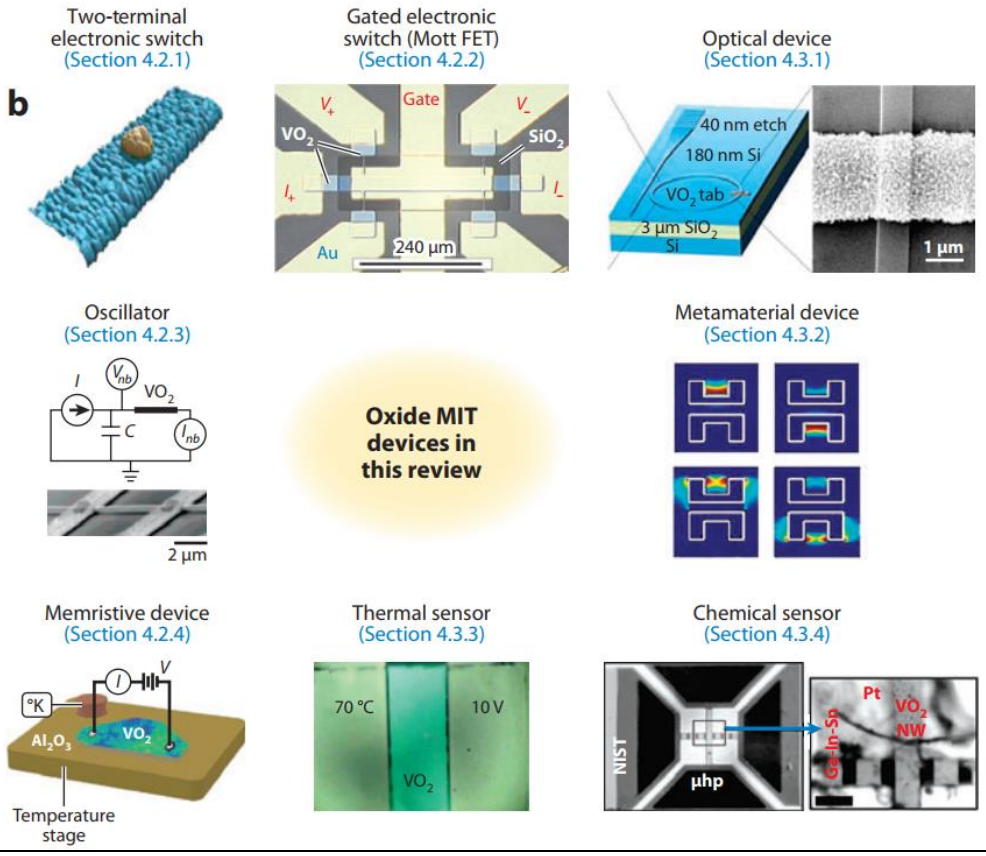

Fig. 3. Devices based on MIT [11].

In VO_2 at a critical temperature (T_c) of about 340 K and normal pressure, MIT of the first order occurs. For monocrystals, the resistance changes by almost 5 orders of magnitude. At the same time, the symmetry of the crystal lattice changes: a transition to a tetragonal lattice (of the rutile type) from the monoclinic lattice, and the volume of the unit cell decreases by half, which corresponds to the Peierls transition. For a long time it was believed that it was Peierls PT caused the MIT in VO_2. Recently, many papers have appeared, in which it was shown that the MIT in VO_2 can be the Mott's PT associated with the interelectron interaction, and the structural transition is a secondary phenomenon accompanying the electronic MIT. VO_2 among the oxides of metal oxides occupies a special place, since vanadium is an element with an uncomlet d-shell, and therefore the strong correlational effects appear in VO_2. Because of these electronic correlations, VO_2 has unique properties, including those associated with a variety of types of chemical bonds between oxygen and vanadium atoms, including bonds due to d-electrons. Therefore, the studies of MIT in VO_2 are of considerable interest in terms of fundamental research, since it is a model object for highly correlated materials and systems. See Fig. 4 as an illustration of modern ideas about MIT in VO_2. On the other hand, VO_2 is a material which is considered as very promising for applications. MIT in VO_2 can occur under the influence of various external influences: under the influence of temperature, electric field (current and voltage), electromagnetic waves (EMW), mechanical stress etc. [12-20].

An important feature of MIT in VO_2 is that, in the case of optically induced MIT, the transition occurs on a superfast time scale [12, 17, 21, 22]. Namely, the speed of this PT reaches the order of hundreds of femtoseconds, which can become a very important factor for applications [12, 17, 22]. It should be noted that among many important tasks, temperature control and PT speed has a very high priority, since the areas and functionality of MIT applications in VO_2 strongly depend on these two parameters. The work in this direction is conducted see [12-20].

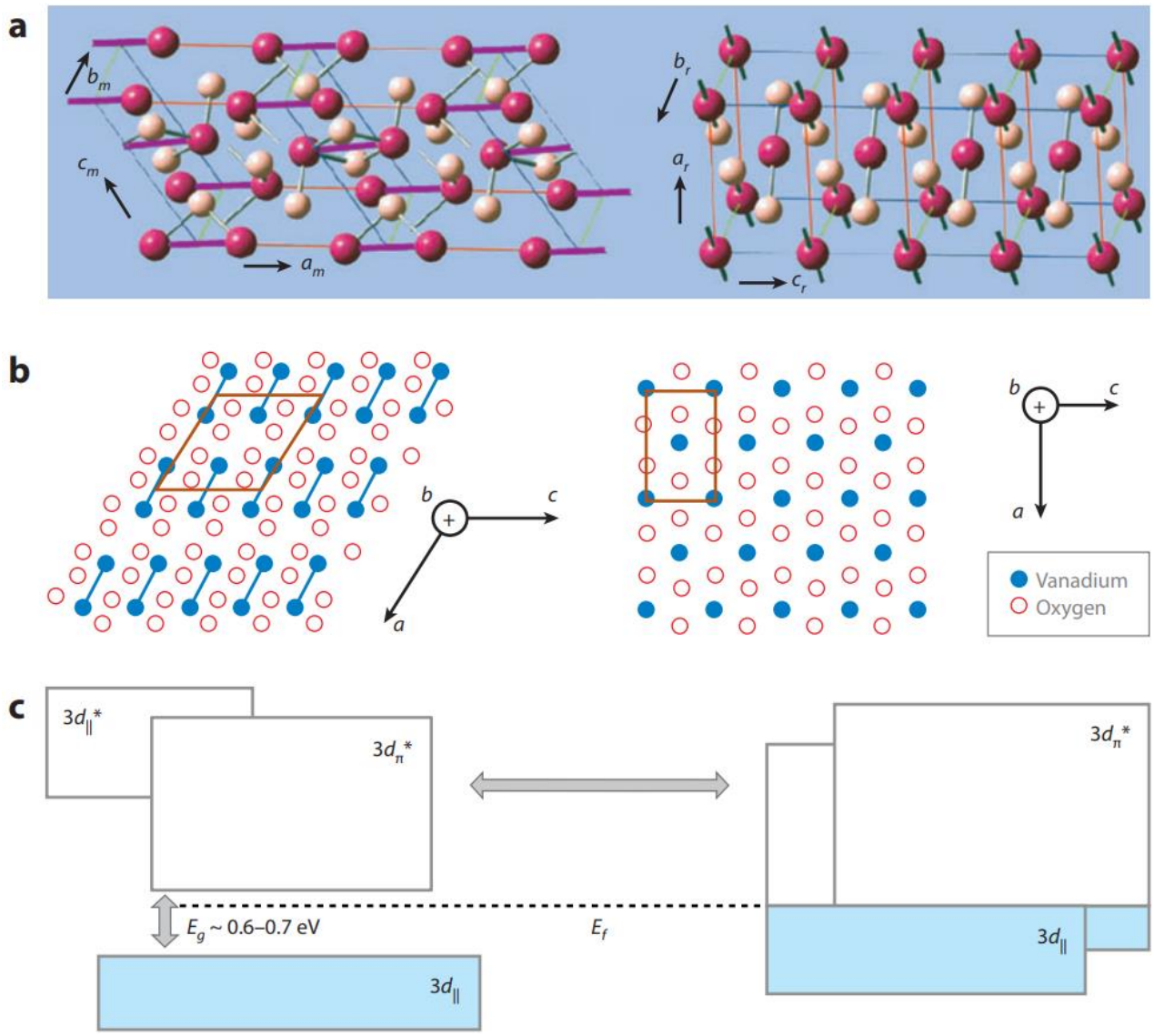

Fig. 4. Structure and band diagram of VO_2. (*a*,*b*) Structure change of VO_2 from the monoclinic insulating phase (*M*1) to the tetragonal rutile metallic phase (*R*) during MIT in (*a*) a three-dimensional view and (*b*) a crosssectional view. (*c*) Band structure change of VO_2 across the MIT. The left and right panels show the band structures for the insulating and metallic phases, respectively [11].

The next most important parameters related to the possible applications of MIT in VO_2, are dimensional effects and especially the possibility of observing MIT in VO_2 on a nanoscale of dimensions, since all the applications studied in this project related to controlled NAs, nanophotonics, etc., are related precisely to the possibility of implementing an MIT exists in VO_2 on a nanoscale. In this regard, it should be noted that recently a number of papers have appeared, in which it was shown that MIT is also observed at nanosized samples of VO_2 [24-29]. Moreover, it was shown

in [25] that the temperature of the MIT can be reduced by changing the dimensions from 340 K in a bulk sample to 302 K in nanowires.

As it was already noted, at MIT in VO_2, there is a huge change in resistance, which means that it must cause a change in the complex dielectric constant, and, consequently, in impedance and reflectance and other electromagnetic properties over the entire wavelength range. Thus, at a temperature higher than T_c of MIT, VO_2 has a metallic conductivity with a carrier density of ~ 10^{22} cm^{-3}, while the optical refractive index varies greatly, from 2.5 in the monoclinic phase to 2.0 in the tetragonal phase. MIT in VO_2 is accompanied by a sudden increase in the reflection coefficient (R) of electromagnetic radiation. This jump of R, is related to the change in the complex dielectric permittivity $\varepsilon = \varepsilon_1 - i\varepsilon_2$, which at the normal incidence of the EMW is determined by the expression [30]:

$$R = | (\sqrt{\varepsilon}-1 - \sqrt{\varepsilon}-2) / (\sqrt{\varepsilon}-1 + \sqrt{\varepsilon}-2) |^2 \quad (1)$$

The increase in the reflection coefficient is due to a sharp increase in the conductivity σ (T) = $\omega\varepsilon_2$ (T) / 4π and the imaginary part of the permittivity ε_2 with temperature (ω is the frequency), provided that the real part of the permeability is small and $\varepsilon_1 \approx \varepsilon_2$. A few papers have been devoted to the study of electromagnetic properties in the microwave range in VO_2 near MIT [21 - 27]. So in Ref. [22] the reflection of microwave electromagnetic radiation during the MIT in VO_2 is considered. It is shown that, with electromagnetic excitation on microwaves in VO_2 and its dielectric composite materials, the reflection coefficient at the MIT of the dielectric state into the metal can be tested to test both a jump-like increase and a decrease. The amplitude of the change depends on the frequency of the field and the thickness of the sample. The behavior of the reflection is due to a change in the conditions for the interference of the reflected waves during MIT. Also in many articles [31-36] of an applied nature, an experimental and theoretical study of the microwave properties of VO_2 with MIT is carried out. So scattering parameters, including reflection, attenuation as a function of frequency and temperature, the dependence of these quantities on the phase state of VO_2 was established [32-36].

Such bright effects of the interaction of VO_2 with EMW could not but cause recently a flow of works devoted to the creation of controlled metamaterials and metasurfaces based on MIT in VO_2 [37-47], in which various types of metamaterial structures and their properties in different wavelength ranges are studied. So in [45] metamaterials based on surface plasmon resonance (SPR) from gold and VO_2 frequency range 8 ~ 12 GHz are considered, transmission and absorption spectra for various input powers are measured. In this paper, it is shown that the metamaterials studied on the basis of VO_2 demonstrate the ability to reconfigure electromagnetic properties in the X-band.

Also in similar metamaterials based on the SPR in VO_2 for the IR band Raman scattering was investigated [46]. At the same time, the wavelength of the electrical resonance showed a blue shift of about 73 nm, while the magnetic resonance regime had a redshift of about 126 nm near MIT. It was also found that with MIT in VO_2, both the electrical and magnetic modes of shear are hysteresis. It has been demonstrated that in the case of using these active metamaterials in tunable Raman scattering (SERS) for a fixed wavelength of the exciting laser, the Raman scattering intensity can be significantly changed by adjusting the frequency of the electric SPR mode, which is achieved by controlling the phase VO_2 by means of precise temperature control.

Of interest is also the paper [47], in which the switching by MIT in VO_2 in chiral metamaterials was studied. The thermal control of chiral switching in a hybrid metamaterial in THz with a modulation depth of 96.6% in the frequency range of about 1.4 THz for linear transverse polarization transmission was demonstrated in Ref. [47].

The next very interesting topic is controlled NAs based on MIT in VO_2, to which much less articles are devoted. So in [48] it considered a very interesting metamaterial based on gold micro and NAs on a substrate of VO_2 for the spectral range 0.2-2 THz. In [49] broadband modulation of terahertz (THz) radiation is experimentally realized by electrically controlled MIT VO_2 in devices with a hybrid metal antenna-VO_2. Devices consist of the active layers of VO_2 and antenna arrays.

As a result, a terahertz wave with a large beam aperture (~ 10 mm) can be modulated in wide spectral range (0.3-2.5 THz) with a frequency independent modulation depth of up to 0.9, which opens the way to the realization of multifunctional components for terahertz applications. In [50], the passage of a THz signal through a VO_2 film with NAs representing a nano-pattern from an array of ordered NAs is studied. Each antenna has a length of 150 μm, and the width varies from 120 nm to 2.5 μm. The antennas are separated by a distance of 10 μm in the vertical direction, and the period is 30 μm in the horizontal plane. It is shown that such a size of the elements of the array of NAs affects the temperature of the PT in the VO_2-film.

It would also worth noting that in 2008, self-oscillations of the current and voltage in the VO_2 film were discovered in an electrical circuit that did not contain any reactive components [51, 52]. The circuit included only a constant voltage source, a polycrystalline VO_2 film and a series resistance. Self-oscillations consisted in a periodic, with a frequency of up to 1 MHz, changes in the values of voltage and current passing through the VO_2 film. At present, it is assumed that in self-oscillations, the entire volume of the VO_2 film alternates from the semiconductor state to the metallic state, and the switching from one state to the other occurs under the action of an electric field by the Mott mechanism without a significant change in the film temperature. Within the framework of this model, it is difficult to explain why mean electrical resistance of a VO_2 film under self-oscillations changes by no more than 1-2 orders of magnitude, while the electrical resistance of a semiconductor state differs from that in a metallic state by 2-3 orders of magnitude. Perhaps this indicates the existence of not yet recognized structural phases or unknown kinetic effects accompanying MIT.

In particular, the use of oxides films for manufacturing ultrafast FETs, optical modulators, gas sensors, solar cells, hydrogen fuel cells, etc. is being studied. At the same time, the number of publications devoted to simple oxide films has increased more than tenfold over the years. In particular, the number of works on the use of oxide films in electronic devices operating in the frequency range from 0.3 to 10 THz has increased. These include modulators, switches, filters, etc. In this range lie the

emission spectra of astronomical objects, as well as spectra of complex organic molecules. Terahertz radiation is harmless to human health, which allows it to be used for medical diagnostics, in modern security systems, environmental monitoring, for quality control of medicines and food products.

A large scientific interest is directed to the study of VO_2 [53- 66] whose single crystals, with dielectric properties, have a high transparency and low absorption due to a low concentration of free carriers (~ 1018 cm^{-3} at f < 6.7 THz) [1]. At a temperature of T_c = 340 K [53,60] VO_2 undergoes MIT in which a monoclinic crystallographic structure is transformed into a tetragonal crystalline structure [53-69]. It was noted in Ref. [64] that when the film is illuminated with a laser pulse with a dose of 0.15 mJ/cm^2, switching occurs for 8 ps. When using a pumping laser with a dose of 2.0 mJ/cm^2 for pumping, the switching time lies in the range of several hundred femtoseconds [56]. This transition is characterized by a hysteresis effect [60]. The transition is accompanied by a sharp change in the optical properties in the terahertz and infrared spectral ranges [70-72]. The decrease in the transmission coefficient over a wide frequency range from 0.3 to 2.5 THz can be more than 80% [53]. At the same time, the reflection coefficient R significantly increases [63].

On the basis of the above review, we formulate the objectives of the work: produce samples of VO_2 films and study their properties in the EHF (8 mm) ranges both in reflected and intrinsic radiation modes that are of greatest interest. To make prototypes of NAs, micro-holes, and slots, as well as to study their interaction with EMW in the visible range using Raman scattering methods. Finally, the optical characteristics of VO_2 nanosphere and also temperature effect on these characteristics are investigated theoretically. The obtained results demonstrate that individual VO_2 nanosphere experiences LSPR at about 1000 nm which can be switched thermally.

2. Experiment

The samples of the VO_2 thin film (370 nm thickness) was obtained using a modernized set up UVN-71 (equipped with a flat axial magnetron), using a reactive magnetron sputtering method in direct current in argon and oxygen. The deposition

time of the film is 40 minutes (on a fixed substrate of SiO_2, 1.53 mm thickness), and the target-substrate distance is 80 mm.

On the obtained VO_2 films for modeling the properties of NAs, nano holes of submicron size, aperture and slit matrix (see Fig. 5) were fabricated using the focused ion beam (FIB) device FEI FIB Strata 205.

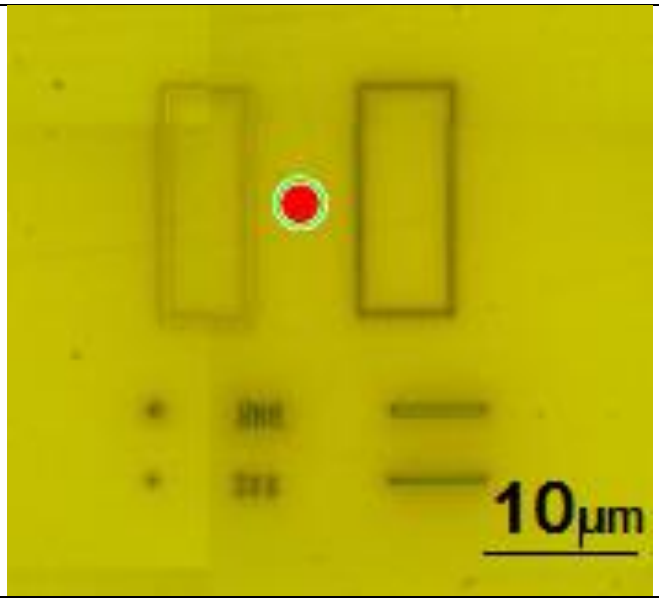

Fig. 5. The holes, hole matrixes, and slots produced by FIB milling in VO_2 - 370 nm thickness film on SiO_2 substrate.

To solve the problem of measuring the intrinsic radiation of a sample of a VO_2 film under MIT in vacuum or air, an installation is designed to measure radiation in the range of 8 mm of samples during thermal cycling in the temperature range from 273 to 393 K (Fig. 6). The installation works as follows. The sample (4) undergoes a PT as a result of heating and cooling by a Peltier element (6), the sample temperature being controlled by a thermocouple (5). Not only the sample (4), but also the radiometer is the source of thermal radiation. The thermal radiation generated by the radiometer is fed into the waveguide (8 mm) and through the circulator (1) falls on the cooled load (black body) (3). Radiation of a load cooled by liquid nitrogen (less intense than the radiation of the radiometer) through the attenuator (2) and the circulator (1) falls on the sample (4). The attenuator (2) regulates the relationship between the "cold" radiation of the load and the "warm" room radiation incident on the sample. This radiation is partially reflected from the sample and gets back into the radiometer along with its own radiation.

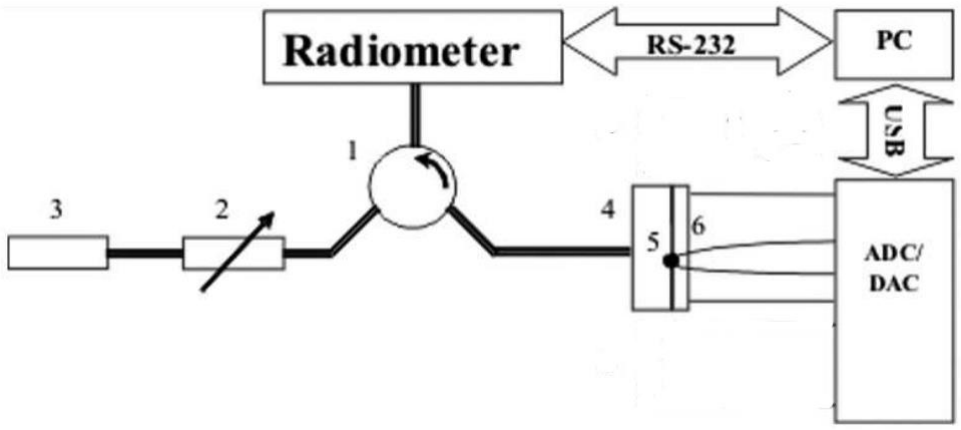

Fig. 6. Scheme of installation for the study of phase transitions by using radiometer with a 28-32 GHz band: 1 – the circulator; 2 – the attenuator; 3 – the cooled load (blackbody); 4 – the sample VO_2 thin film; 5 – the thermocouple; 6 – the Peltier element.

The intrinsic emission of a thin film VO_2 near the MIT (T_c = 340 K) was experimentally studied in the 8 mm range. A diagram of the installation of the sample near the waveguide is shown in Fig. 7. Contributions from the intrinsic and reflected radiation are separated by a difference measurement technique. The sample was irradiated with illumination of different brightness temperature: from 90% to 0% of the "cold" radiation from the load - a blackbody cooled by nitrogen. The ratio of "cold" and "warm" radiation was regulated on the attenuator. In the presence of "warm" room radiation (nitrogen load 0-70%), the signal level on the radiometer grows linearly with temperature, and in the region of MIT there is a sharp increase in intensity by 15% and temperature hysteresis (Fig. 8). The intensity of these anomalies of radiation (in absolute value) in VO_2 with PT, fixed by the radiometer, does not change with increasing brightness temperature of the illumination from the boiling point of liquid nitrogen to RT. In the previously studied metallic alloys with structural Ni-Mn-Ga-Fe [73] and Ti-Ni-Cu [74], the intensity of radiation anomalies recorded by the radiometer decreased with increasing brightness temperature of the illumination, which indicates the different nature of the intrinsic radiation at PT in metallic alloys of Ni-Mn-Ga-Fe, Ti-Ni-Cu and thin VO_2 films (see Fig. 8).

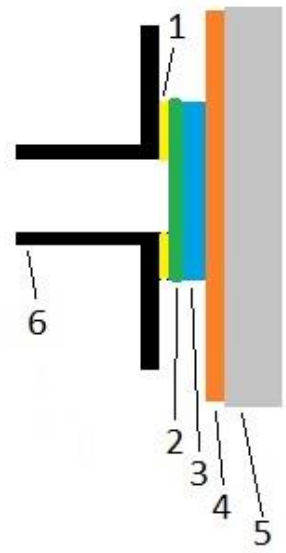

Fig. 7. Schematic representation of the sample installation near the waveguide 8 mm, top view: 1 – the heat-insulating layer of cardboard; 2 - the sample VO_2 thin film (370 nm); 3 – the substrate of SiO_2 (the thickness of 1.53 mm); 4 – the copper plate; 5 – the Peltier element; 6 – the waveguide 8 mm.

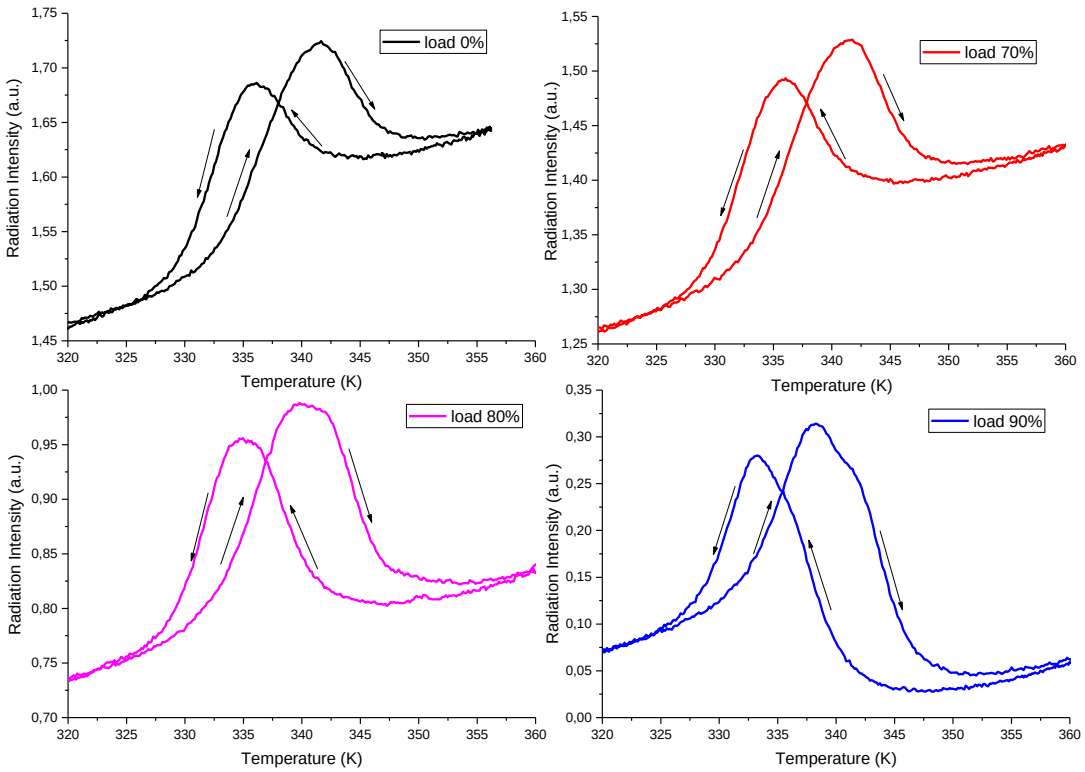

Fig. 8. Temperature dependence of the radiation intensity of the sample, taken on a radiometer with a nitrogen load: from 90% down to 0% of the "cold" radiation from the load – the blackbody cooled by liquid nitrogen. The ratio of "cold" and "warm" radiation is regulated by the attenuator.

To measure the reflection coefficient of the VO_2 samples near the MIT, a standard panoramic sweep-frequency reflectometer P-2 series with rectangular standard waveguides at frequencies of 27-37 GHz was used. The scheme of the experiment is shown in Fig. 9, in which: 1 - the oscillating frequency generator; 2 – the directional coupler and detector head of the incident wave; 3 – the directional coupler and detector head of the reflected wave; 4 – the investigated object - VO_2 thin film; 5 – the indicator unit of panoramic sweep-frequency reflectometer.

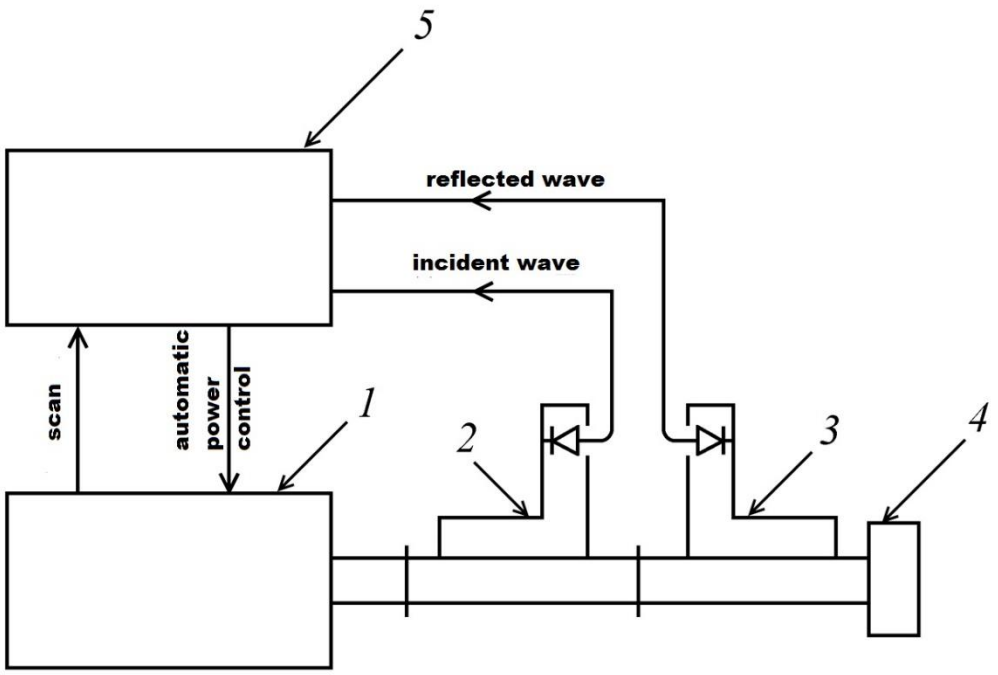

Fig. 9. Block diagram of the installation for measuring the reflection coefficient: 1 – the oscillating frequency generator; 2 – the directional coupler and detector head of the incident wave; 3 – the directional coupler and detector head of the reflected wave; 4 – the object under study; 5 – the indicator unit of VSWR.

The Raman scattering spectra were studied using model NAs specially prepared using the FIB method - holes, hole matrixes, and slits. Raman spectra were obtained with the help of the Raman spectrometer Senterra from Brucker. To excite the Raman spectrum radiation, a laser with a wavelength of 532 nm and a variable power of 2-20 mW was used. The accumulation time of the signal at the point was 15 times per 25 s. After subtraction of the background, the spectra were normalized. In the case of VO_2, whose properties depend on the phase composition, it is possible to observe the effects of the power of the laser incident radiation on the measured spectra (see Chapter 3.2).

3. Results and discussions

3.1. Properties of VO_2 films in EHF range

In Fig. 10 shows the reflection coefficient of VO_2 in the range 27-37 GHz on the panorama indicator at different temperatures in the vicinity of the dielectric-metal PT in a thin VO_2 film: below the PT at 331 K, near PT at 340 K and above PT at 345 K. Also with this method the hysteretic behavior of the reflection coefficient of the VO_2 film is shown for direct and inverse MIT, while the shape of the curve depends strongly on the frequency (Fig. 11). To explain the frequency dependence of the reflection coefficient, a theoretical model has been proposed within the framework of the Drude theory, since the optical characteristics of VO_2 undergo significant changes in PT [75].

331 K	340 K	345 K

Fig.10. The reflection coefficient in the range 27-37 GHz on the VSWR indicator at different temperatures in the vicinity of the MIT in a thin VO_2 film: lower - 331 K, near - 340 K and above - 345 K.

It was found that a thin film of a material on a glass substrate with a shielding layer of a conductor placed in a rectangular microwave waveguide could show features in the frequency dependence of the reflection coefficient of EMW at temperatures close to the PT temperature. The investigated structure of VO_2 is glass-copper (Fig. 7). Copper is considered to be perfectly conductive (everything is reflected), quartz does not have frequency dispersion and the dielectric constant (ε = 3.8 for SiO_2 [75]) does not change with temperature. VO_2 is modeled in the framework of the Drude theory: the plasma frequency and the collision frequency of electrons depend on the temperature [76]. Substrate SiO_2 thickness is equal to 1.53 mm, the VO_2 film thickness is equal to 370 nm. For estimating calculations, we shall consider the temperature dependence to be piecewise continuous (see Fig. 12). The

approximation is rough, but suitable for qualitative description. The results of the calculations are shown in Fig. 13. It can be seen that the qualitatively temperature dependence of the reflection coefficient satisfactorily describes the measurement results.

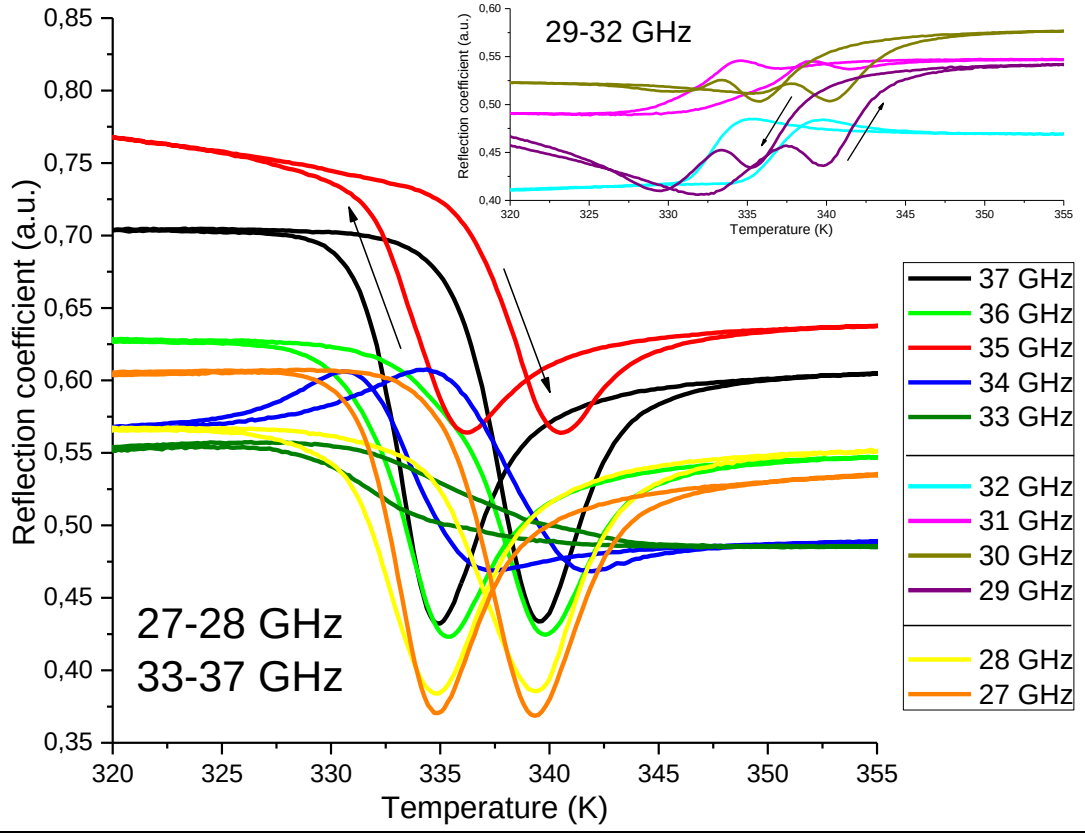

Fig. 11. Temperature dependence of the reflection coefficient, recorded on a panoramic reflectometer at different frequencies from 27 to 37 GHz.

In general, the main problem in the theoretical description is the preservation of the dip in the temperature dependence of the reflection coefficient in the frequency range 30-35 GHz, which disappears in the experiments (Fig. 11). The dip seems to be related to the excitation of plasmon resonance in the VO_2 film: the plasma frequency increases and at a certain temperature becomes comparable with the frequency of the EMW in the waveguide. This is indirectly confirmed by the fact that the temperature of the dips in Fig. 13 increases with increasing frequency (plasma frequency also increases with temperature). The width and depth of the depressions depends mainly on the collision frequency of the electrons. Therefore, the disappearance of the dips may be due to the fact that the collision frequency in the VO_2 samples becomes comparable or greater than the frequency of the EMW. Such values are also achieved

in Fig. 12, but it is necessary that these values should be at the same temperatures when plasmon resonance occurs.

Recently, a photoinduced PT has been experimentally observed at temperatures below the PT temperature in the absence of material illumination by a medium-infrared laser (the photon energy is close to the width of the forbidden band) [27, 28]. Earlier, the possibility to initiate a PT by terahertz radiation (photon energy much less than the band-gap width) in a VO_2-based metamaterial was experimentally demonstrated [29]. While in the latter case, the PT is related to the Joule heating loss to the PT temperature, in the first case, at the present time, a satisfactory model describing the PT is still not developed.

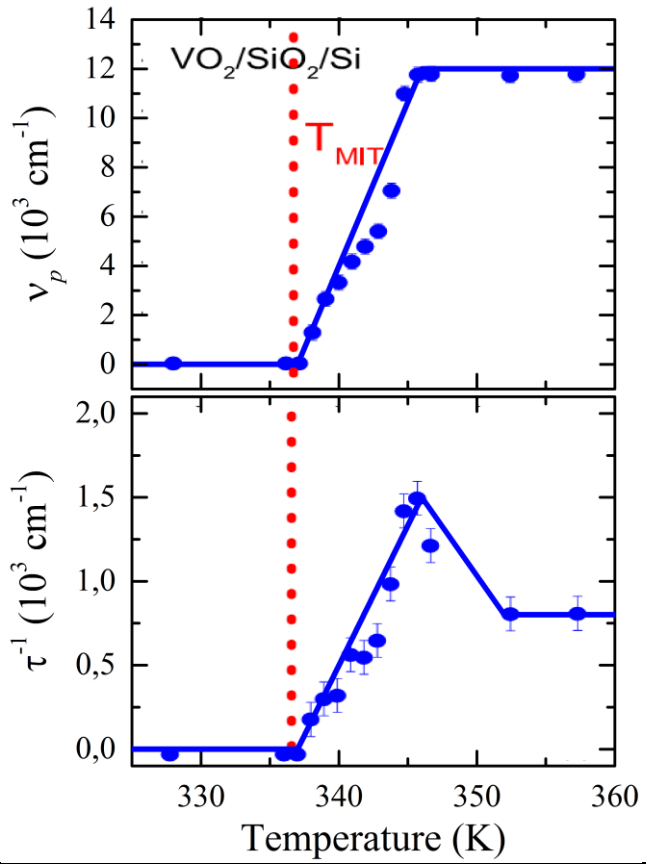

Fig. 12. Temperature dependence of the plasma frequency $\upsilon_p=\omega_p/2\pi$ and the electron collision frequency in the VO_2 film: the experimental results are denoted by markers [76], and the solid lines are piecewise-continuous approximation.

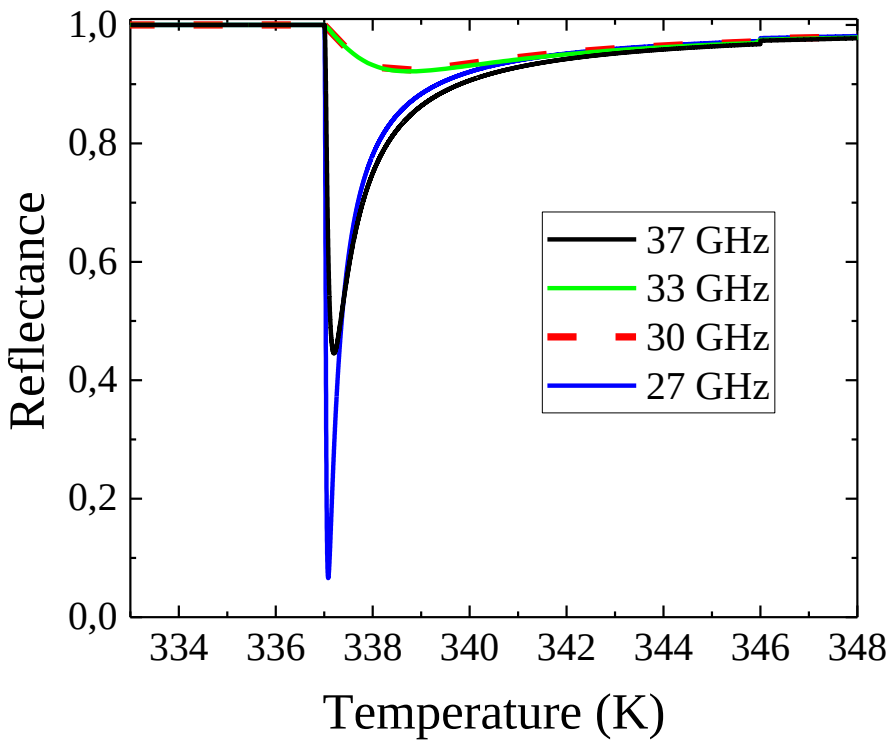

Fig. 13. Temperature dependence of the reflection coefficient in the frequency band 27-37 GHz at heating (model calculation).

3.2. Raman spectra of NAs based on VO_2

The spectra obtained from the structure formed by two adjacent holes in the VO_2 film and the surface of the film after subtraction of the background and normalization show differences: the relative intensity of the 620 cm^{-1} peak obtained in the region of the bridge between the holes is much smaller than that of the analogous peak in the spectrum, obtained on the film (Fig. 14). There is also a shift toward smaller wave numbers at the peak obtained from the web (614 and 622 cm^{-1} in the region of the web and the film, respectively). This behavior of the peak is possibly related to the compression voltage that has arisen in the region of the jumper.

Fig. 15 shows the spectra obtained after irradiating the surface of the VO_2 film with laser radiation of different power (2, 10, and 20 mW). On the spectrum obtained after irradiation with a laser of 20 mW, it is seen that there are additional peaks 146, 284, 531, 703 and 997 cm^{-1}, compared with the unirradiated one. The appearance of these peaks may be due to photoinduced production of the V_2O_5 phase [80].

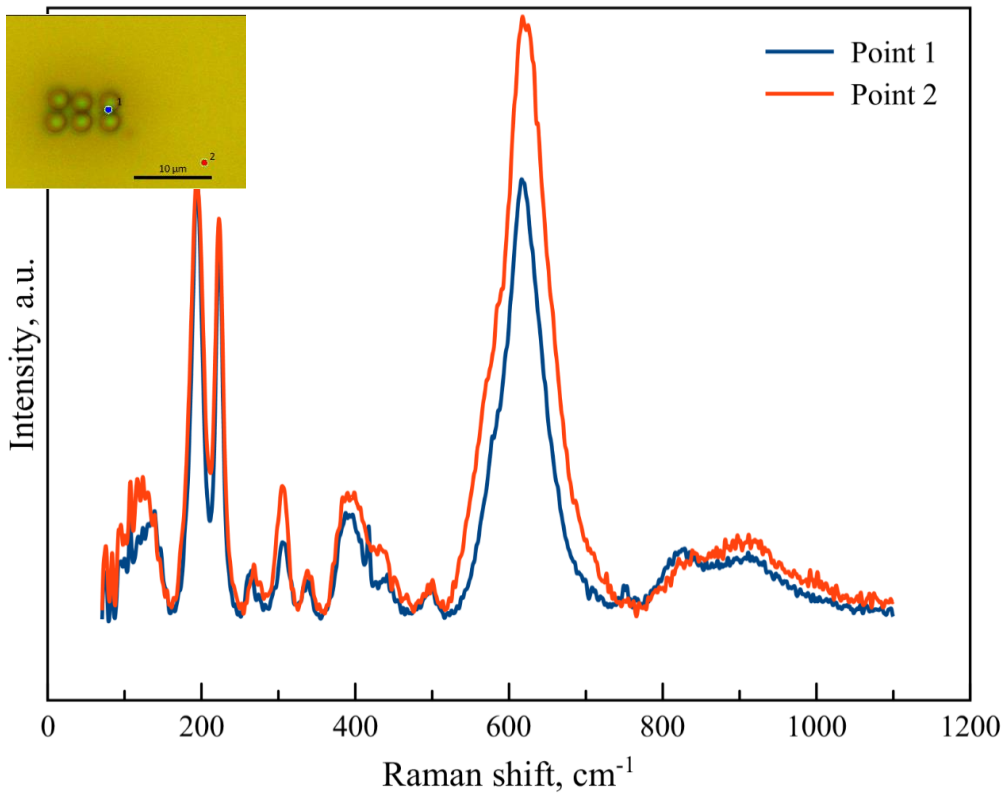

Fig.14. Raman Spectrum shift from VO_2 sample defined in inset in the border of a hole (Point 1) and in the film surface (Point 2).

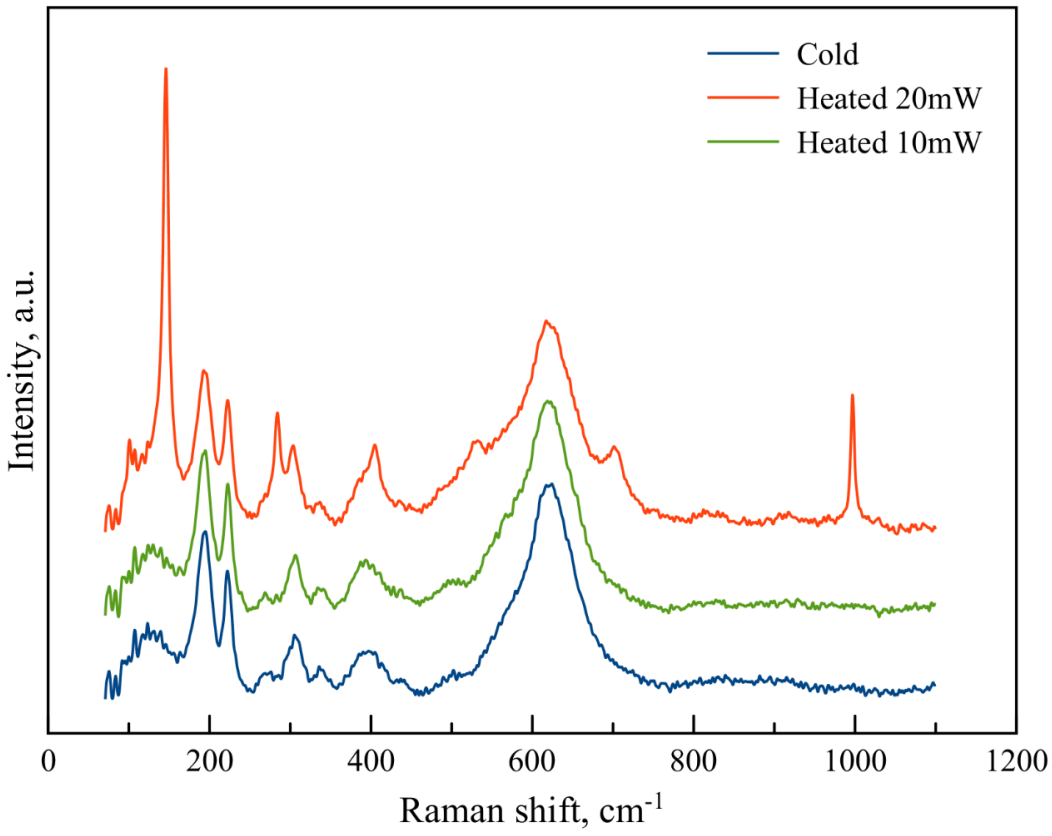

Fig 15. Raman spectrum shift of VO_2 film before heating (cold), after laser irradiating with 10 mW laser power (heated 10mW) and after laser irradiating with 20 mW laser power (heated 20mW).

3.3 Properties of VO_2 nanosphere in optical spectrum

In this paper, optical properties of VO_2 nanosphere are studied theoretically by exploiting various methods such as dipole approximation (DA), modified long wavelength approximation (MLWA) and Mie theory. In order to investigate temperature effect on these characteristics, the temperature dependent dielectric constant of VO_2 are extracted from experimental data in [81]. It is noteworthy that the Drude model is not capable in visible and near infrared range [82]. The nanosphere is surrounded by air in simulations.

3.3.1 Dipole approximation

Optical responses of a VO_2 nanosphere with optical constant $\varepsilon = \varepsilon_1 + i\varepsilon_2$, immersed in a medium with permittivity of ε_m are simply computed by dipole approximation. Notice that the dimension of nanosphere must be much smaller than wavelength (>1% wavelength). The real (ε_1) and imaginary parts (ε_2) of VO_2 dielectric constants above and below the T_c are shown in Fig.16. By applying this method, the absorption, scattering and extinction cross sections are expressed respectively as follow:

$$C_{\text{abs}} = k\,\text{Im}\{\alpha\}, C_{\text{sca}} = \frac{k^4}{6\pi}|\alpha|^2, C_{\text{ext}} = C_{\text{abs}} + C_{\text{sca}} \quad (2)$$

where k is the wave number and α is polarizability coefficient of nanosphere obtained by ($\alpha = 4\pi a^3 \frac{\varepsilon - \varepsilon_m}{\varepsilon + 2\varepsilon_m}$) [83]. The parameter a is the radius of nanosphere. The dimensionless optical efficiencies are computed as follow:

$$Q_i = \frac{C_i}{A} \quad i \in \{\text{abs}, \text{sca}, \text{ext}\} \quad (3)$$

in which A is geometrical cross section illuminated by incident light. This parameter corresponds to πa^2. The polarizability experiences a resonant enhancement when the ($|\varepsilon + 2\varepsilon_m|$) is minimized, which for the small or slowly varying ε_2, simplifies to $\varepsilon = -2\varepsilon_m$ (Fröhlich condition) [84]. This enhancement is observed in metallic phase

of VO_2 nanosphere (355 K). In this case, the real part of dielectric constant becomes negative as can be seen in Fig. 16.

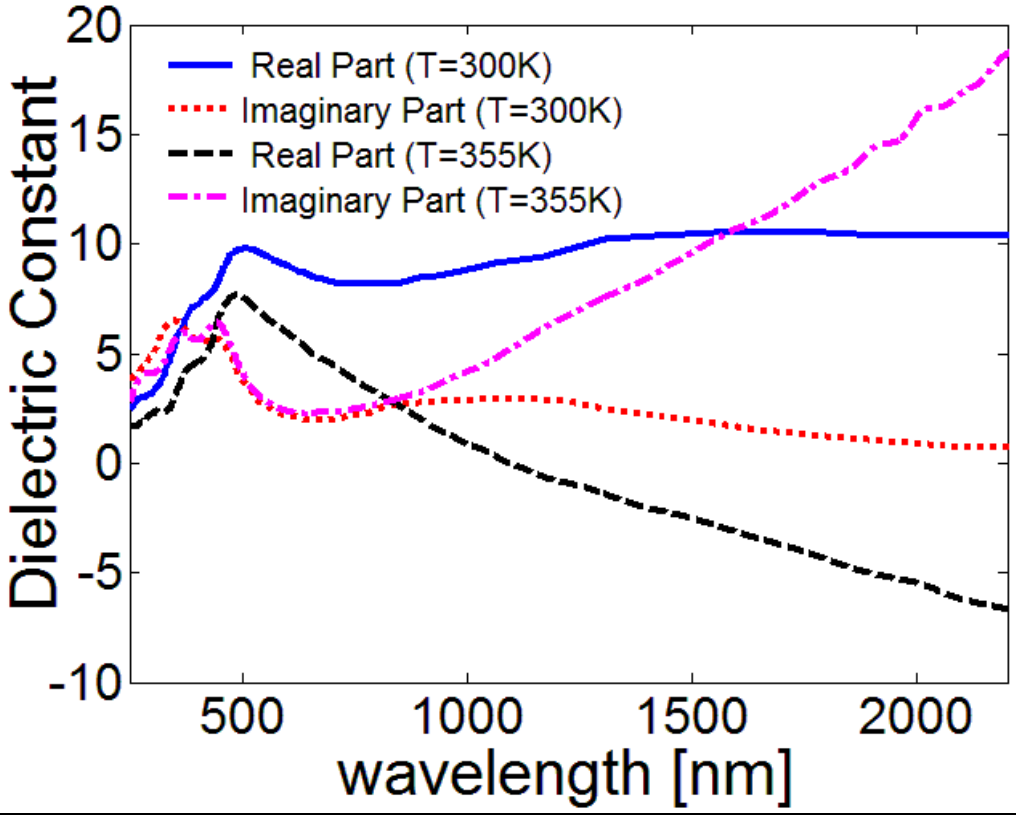

Fig 16. Experimental dielectric constant of VO_2, below and above the T_c, extracted from [81].

3.3.2 Modified Long Wavelength Approximation

As the radius of nanospheres increases, DA loses its accuracy and is not applicable. However, by using modified polarizability ($\tilde{\alpha}$), DA can be utilized for the nanospheres in which dimensions are less than 10% of wavelength. By calculating $\tilde{\alpha}$ the optical cross sections and efficiencies can be obtained by prior equations. The modified polarizability is expressed as $\frac{\alpha}{1-\frac{2}{3}ik^3\alpha-\frac{1}{a}k^2\alpha}$ [85].

3.3.3 The Mie theory

The Mie theory is a powerful method in computing optical properties of nanospheres. In this procedure, electromagnetic fields are described by spherical harmonics in spherical coordinate. By satisfying the boundary conditions and calculating the scattering coefficients $\{a_n, b_n\}$, optical cross sections are achieved as follow:

$$C_{\text{ext}} = \frac{2\pi}{k^2}\sum_{n=1}^{\infty}(2n+1)\,\text{Re}\left[a_n + b_n\right]$$
$$C_{\text{sca}} = \frac{2\pi}{k^2}\sum_{n=1}^{\infty}(2n+1)\left(|a_n|^2 + |b_n|^2\right) \quad (4)$$

where n is the order of the Riccati-Bessel functions. In order to obtain optical efficiencies, equation (3) is used [83].

The optical efficiencies and electric field distribution of a 20 nm nanosphere in metallic phase are presented in Fig.17 (a,b) and compared with the same dimension Ag nanosphere. There is a resonance around 1000 nm in spectra of VO_2 in metallic phase. Due to the electric field distribution, the origin of this resonance is an electric dipole. The extinction efficiency of a 20 nm Ag nanosphere is shown in the Fig. 17(c). The enhancement in LSPR of Ag is much higher than VO_2 in metallic phase. However, there is a little change in the LSPR of Ag nanoparticle when the particles are heated from RT up to 773 K [86]. It is obvious that the principle of resonance around 1000 nm is the LSP. By lowering the temperature, LSPR disappears; therefore this resonance can be switched thermally as can be seen in Fig.18.

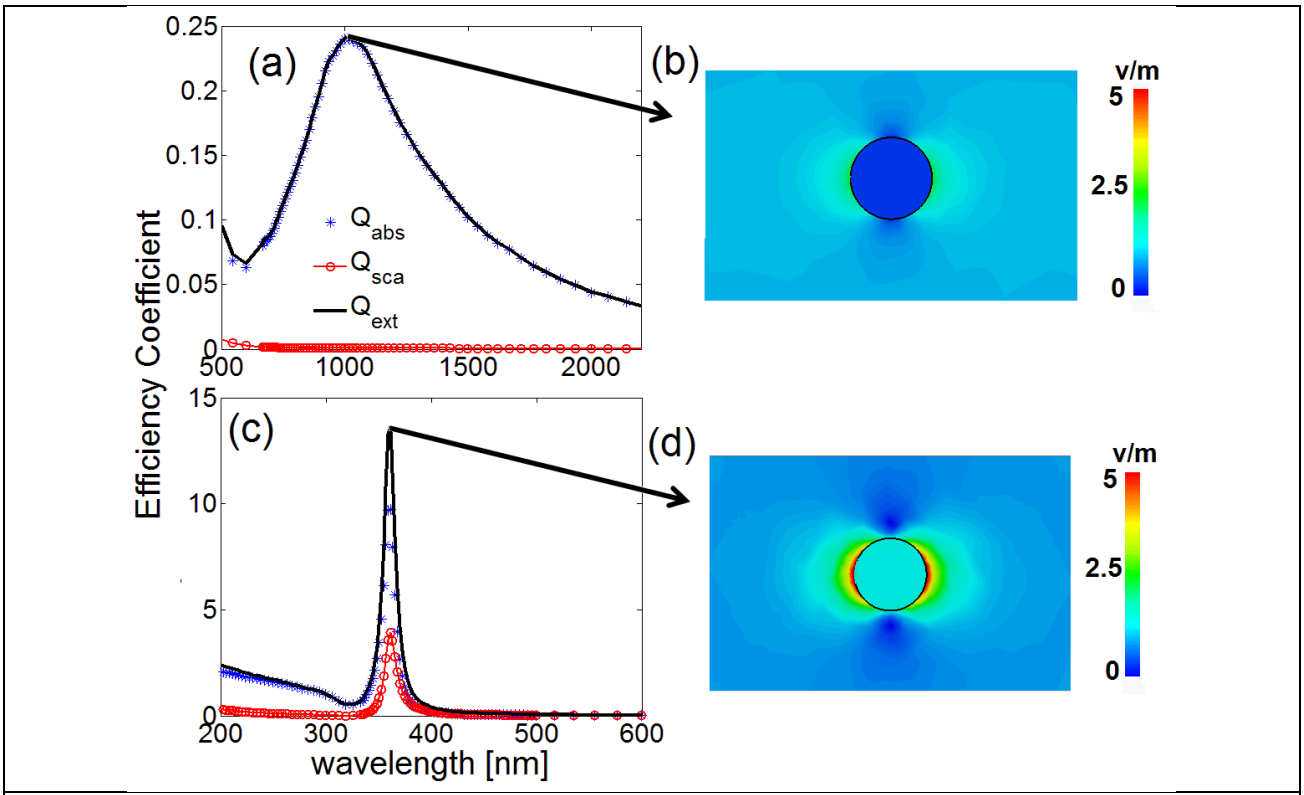

Fig 17. Efficiency coefficients (a) and electric-field distribution (b) of 20 nm VO_2 nanosphere at T=355 K. Optical efficiency coefficients (c) and electric field distribution (d) of 20 nm Ag nanosphere.

The size effect on the optical spectra of VO_2 nanospheres for insulator and metallic phases is investigated. For this reason, the absorption and scattering efficiencies of 20nm, 50 nm and 100 nm are illustrated in Figs. 18-20. According to the obtained results, in the insulator phase (T = 300 K), there is a peak in the optical spectra for 50 nm and 100 nm nanospheres in the visible range. This peak is associated with combined modes. By raising the temperature, VO_2 experiences MIT and becomes metal, conducts to a large absorption and extinction coefficients at the wavelength of 1000 nm for 20 nm nanosphere. The LSPR redshifts and broadens slightly as the radius increases, which occurs in 1011nm and 1064 nm for 50nm and 100 nm nanospheres respectively. This LSPR is obvious in scattering spectra for $r \geq$ 100 nm. More surprisingly, the absorption efficiency is higher than the scattering in the vicinity of the LSPR peaks in all cases.

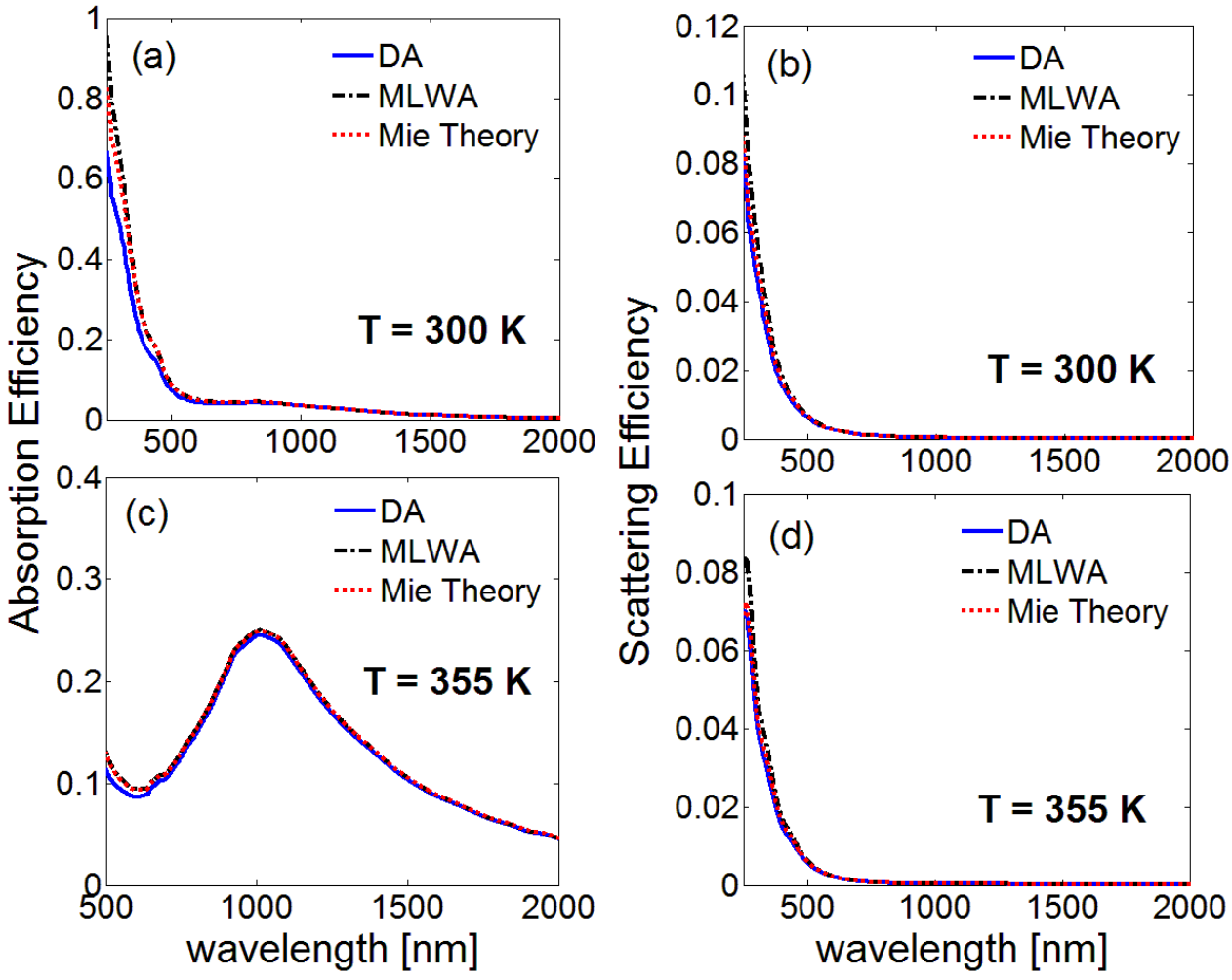

Fig 18. Optical properties of 20 nm VO_2 nanosphere: (a) and (b) at 300 K, (c) and (d) above T_c

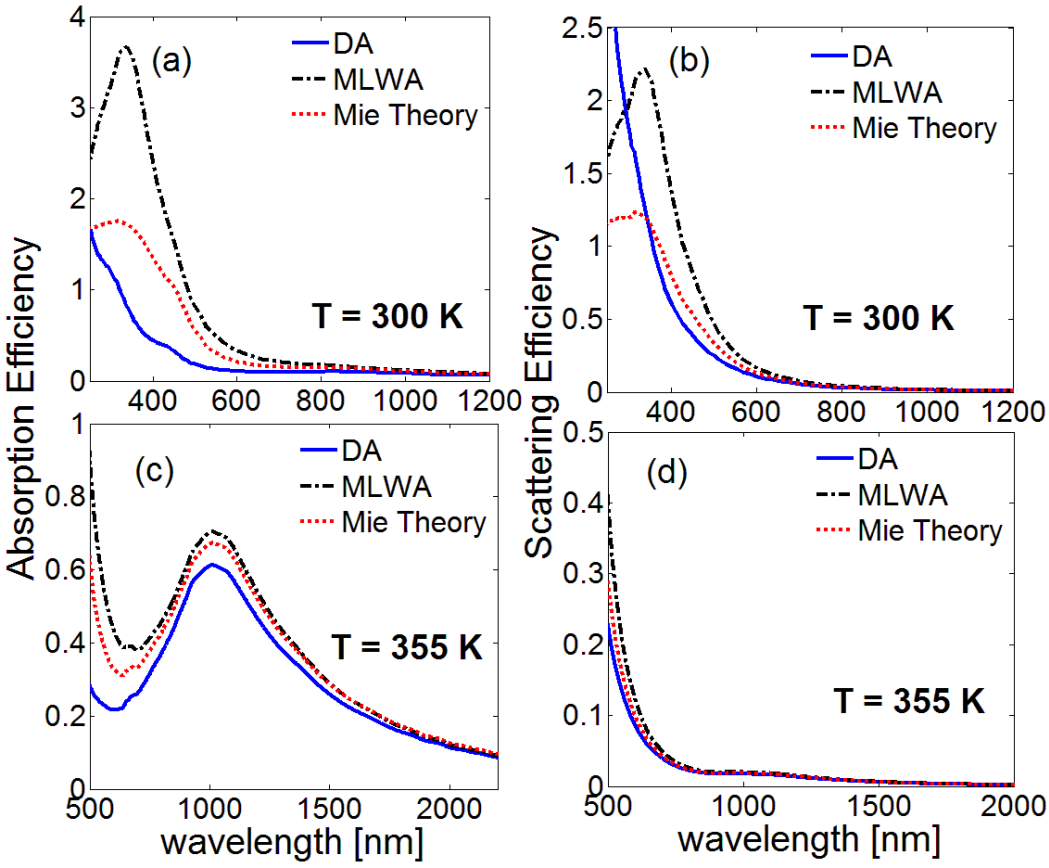

Fig 19. Optical properties of 50 nm VO_2 nanosphere (a) and (b) at temperature below MIT, (c) and (d) above MIT.

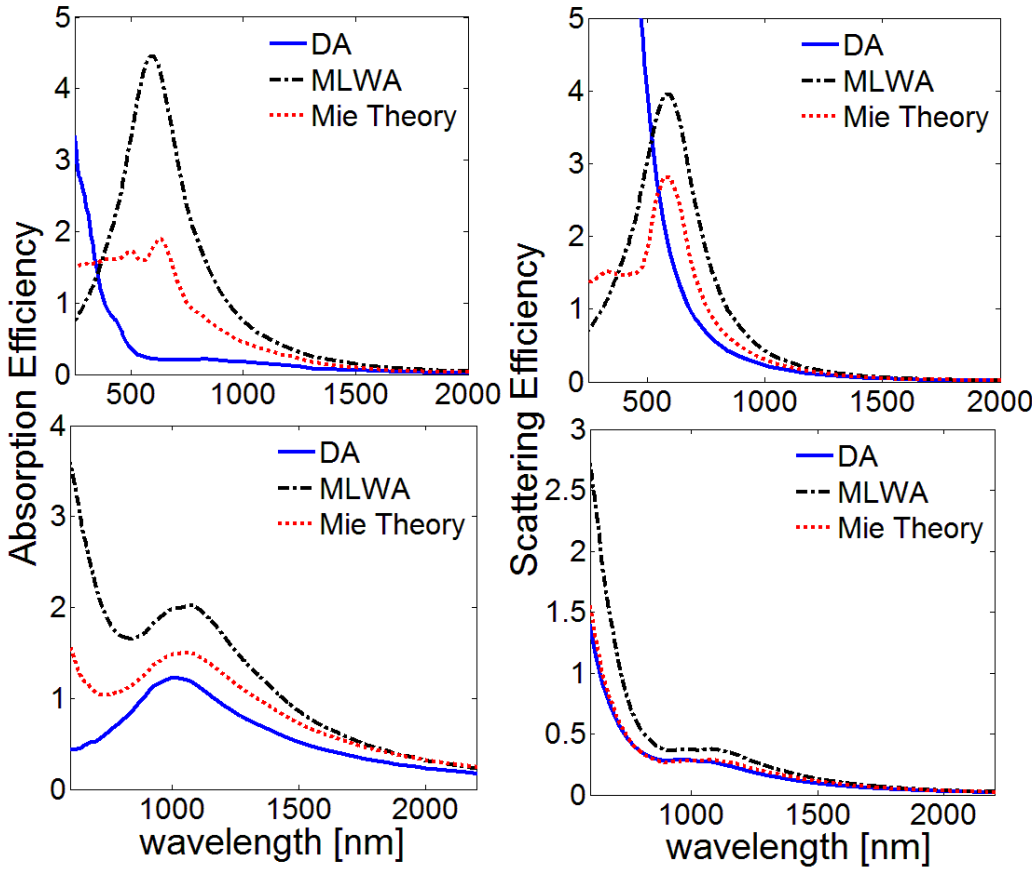

Fig 20. Optical properties of 100 nm VO_2 nanosphere (a) and (b) at temperature below MIT, (c) and (d) above MIT.

4. Conclusion

Thus, the following results can be formulated.

1) The VO_2 films with a thickness of 370 nm were fabricated on a glass substrate. Prototypes of NAs are formed on VO_2 films by the FIB method: micro- and submicron holes, matrixes of holes, and slits.

2) In the study of the transmission coefficient and reflection of millimeter waves from a thin-film structure comprising a VO_2 film and a glass substrate, temperature dependence anomalies were found, which can be explained by a change in the real and imaginary part of the permittivity from temperature at MIT. The reflection coefficient in the 27-37 GHz band was measured at different temperatures in the vicinity of the dielectric-metal FP in a thin VO_2 film: below the PT at 331 K, near the PT at 340 K and above the PT at 345 K. The hysteretic behavior of the reflection coefficient of the VO_2 film was determined for a direct and the inverse MIT while the form of the curve depends strongly on the frequency. To explain the frequency dependence of the reflection coefficient, a theoretical model is proposed in the framework of the Drude theory.

3) The hysteresis features on the temperature dependence of the intrinsic radiation of the VO_2 film in the 8 mm range, related to the direct and inverse MIT of the first kind, revealed by the pyrometric method.

4) In studying the Raman spectrum, the dependence of the VO_2 film spectrum on the laser radiation power was observed. It is concluded that at a laser power of 20 mW, a partial oxidation of the film can occur with the formation of V_2O_5. It is also found that in the region of the film located between the two holes, there are distortions in the spectrum, characteristic of elastically compressed materials.

5) The optical properties of VO_2 nanosphere in insulator and metallic phases, and also size effect on these characteristics have been investigated. VO_2 can switch its LSPR thermally. By increasing dimension of VO_2 nanosphere, the LSPR redshifts slowly and also a peak is observed in optical spectra in insulator case which its origin is combined modes.

Acknowledgments

This work was supported by the Russian Foundation for Basic Research, Grant No. 17-57-560002-Iran_a. T.P. and N.V. acknowledge the support by the Iran National Science Foundation (INSF), grant No. 96003683.

References

1. Zheludev N.I., Plum E. Reconfigurable nanomechanical photonic metamaterials *Nature Nanotechnology*, 2016, Vol. 11, No. 1, P. 16.

2. H.-T. Chen, J.F. O'Hara, A.K. Azad, A.J. Taylor, R.D. Averitt, D.B. Shrekenhamer, W.J. Padilla. Experimental demonstration of frequency-agile terahertz metamaterials. *Nature Photonics*, 2008, Vol. 2, No. 5

3. Y.C. Jun, E. Gonzales, J.L. Reno, E.A. Shaner, A. Gabbay, I. Brener. Active tuning of mid-infrared metamaterials by electrical control of carrier densities. *Optics expres*s, 2012, Vol. 20, No. 2, P. 1903-1911.

4. H.-T. Chen, W. J. Padilla, M. J. Cich, A.K. Azad, R.D. Averitt, A.J. Taylor. A metamaterial solid-state terahertz phase modulator. *Nature Photonics*, 2009, Vol. 3, No. 3, P. 148.

5. H.T. Chen, W. J. Padilla, J.M.O. Zide, A.C. Gossard, A.J. Taylor, and R.D. Averitt. Active terahertz metamaterial devices. *Nature*, 2006, Vol. 444, No. 7119, P. 597.

6. Q. Zhao, L. Kang, B. Du, B. Li, J. Zhou, H. Tang, X. Liang, and B. Z. Zhang. Electrically tunable negative permeability metamaterials based on nematic liquid crystals. *Applied Physics Letters*, 2007, Vol. 90, No. 1, 011112.

7. F.L. Zhang, W. H. Zhang, Q. Zhao, J. B. Sun, K. P. Qiu, J. Zhou, D. Lippens. Electrically controllable fishnet metamaterial based on nematic liquid crystal. *Optics Express*, 2011, Vol. 19, No. 2, P. 1563-1568.

8. V. Stockhausen, P. Martin, J. Ghilane, Y. Leroux, H. Randriamahazaka, J. Grand, N. Felidj, and J. C. Lacroix. Giant plasmon resonance shift using poly (3, 4-ethylenedioxythiophene) electrochemical switching. *Journal of the American Chemical Society*, 2010, Vol. 132, No. 30, P. 10224-10226.

9. J. Berthelot, A. Bouhelier, C.J. Huang, J. Margueritat, G. Colas-des-Francs, E. Finot, J.C. Weeber, A. Dereux, S. Kostcheev, H.I. Ahrach, A. L. Baudrion, J. Plain,

R. Bachelot, P. Royer, G.P. Wiederrecht. Tuning of an optical dimer nanoantenna by electrically controlling its load impedance. *Nano letters*, 2009, Vol. 9, No. 11, P. 3914-3921.

10. W. Dickson, G.A. Wurtz, P.R. Evans, R.J. Pollard, A.V. Zayats. Electronically controlled surface plasmon dispersion and optical transmission through metallic hole arrays using liquid crystal. *Nano Letters*, 2008, Vol. 8, No. 1, P. 281-286.

11. Z. Yang, C. Ko, S. Ramanathan. Oxide electronics utilizing ultrafast metal-insulator transitions. *Annual Review of Materials Research*, 2011, Vol. 14, P. 337-367.

12. S. Lysenko, V. Vikhnin, A. Rúa, F. Fernández, H. Liu. Critical behavior and size effects in light-induced transition of nanostructured VO_2 films. *Physical Review B*, 2010, Vol. 82, No. 20, P. 205425.

13. Chen C., Wang R., Shang L., and Guo. Gate-field-induced phase transitions in VO_2: monoclinic metal phase separation and switchable infrared reflections. *Applied Physics Letter*s, 2008, Vol. 93, No. 17, 171101.

14. Rini M., Cavalleri A., Schoenlein R. W., López R., Feldman L. C., Haglund R. F. Jr., Boatner L. A., and Haynes T. E. Photoinduced phase transition in VO_2 nanocrystals: ultrafast control of surface-plasmon resonance. *Optics Letters*, 2005, Vol. 30, No. 5, P. 558-560.

15. Lysenko S., Rua A. J., Vikhnin V. Jimenez J., Fernandez F., Liu H. Light-induced ultrafast phase transitions in VO2 thin film. *Applied Surface Science*, 2006, Vol. 252, No. 15, P. 5512-5515.

16. Guo H., Chen K., Y. Oh, Kevin Wang, Dejoie C., Syed Asif S.A., Warren O.L., Shan Z. W., Wu J., Minor A. M. Mechanics and dynamics of the strain-induced M1-M2 structural phase transition in individual VO_2 nanowires. *Nano Letters*, 2011, Vol. 11, No. 8, P. 3207-3213.

17. Cavalleri A., Tóth C., Siders C.W., Squier J.A., Ráksi F., Forget P. Kieffer J.C. Femtosecond structural dynamics in VO 2 during an ultrafast solid-solid phase transition. *Physical Review Letters*, 2001, Vol. 87, No. 23, P. 237401.

18. Ilyinskiy A.B., Kvashenkina O.E., Shadrin E.B. Phase transition and correlation effects in vanadium dioxide. *Semiconductors*, 2012, Vol. 46, No. 4, 2012, P. 422–429.

19. Stefanovich G., Pergament A., Stefanovich D. Electrical switching and Mott transition in VO_2. *Journal of Physics: Condensed Matter*, 2000, Vol. 12, No. 41, P. 8837.

20. Zhou Y., Chen X., Ko C., Yang Z., Mouli C., Ramanathan S. Voltage-triggered ultrafast phase transition in vanadium dioxide switches. *IEEE Electron Device Letters*, 2013, Vol. 34, No. 2, P. 220-222.

21. C. Kübler, H. Ehrke, R. Huber, R. Lopez, A. Halabica, R.F. Haglund, Jr., A. Leitenstorfer. Coherent structural dynamics and electronic correlations during an ultrafast insulator-to-metal phase transition in VO_2. *Physical Review Letters*, 2007, Vol. 99, No. 11, 2007, 116401.

22. J. Yoon, H. Kim, X. Chen, N. Tamura, B. Simon Mun, Ch. Park, and H. Ju. Controlling the temperature and speed of the phase transition of VO2 microcrystals. *ACS applied materials & interfaces*, 2016, Vol. 8, No. 3, P. 2280-2286.

23. R. Lopez, T. E. Haynes, L. A. Boatner, L. C. Feldman, and R. F. Haglund. Size effects in the structural phase transition of VO_2 nanoparticles. *Physical Review B*. 2002, Vol. 65, No. 22, P. 224113.

24. Liu H., Lu J., Zheng M., Tang S. H., Sow Ch. H., Zhang X., and Ke L. Size effects on metal-insulator phase transition in individual vanadium dioxide nanowires. *Optics express*, 2014, Vol. 22, No. 25, P. 30748-30755.

25. E.U. Donev, J.I. Ziegler, R.F. Haglund, L.C. Feldman. Size effects in the structural phase transition of VO_2 nanoparticles studied by surface-enhanced Raman scattering. *Journal of optics A: pure and applied optics*. 2009, Vol. 11, No, 12, P. 125002.

26. Appavoo K., Haglund Jr R. F. Detecting nanoscale size dependence in VO_2 phase transition using a split-ring resonator metamaterial. *Nano letters*. 2011, Vol. 11, No. 3, P. 1025-1031.

27. V. R. Morrison, R. P. Chatelain, K. L. Tiwari, A. Hendaoui, A. Bruhács, M. Chaker, B. J. Siwick. A photoinduced metal-like phase of monoclinic VO_2 revealed by ultrafast electron diffraction. *Science*. 2014, Vol. 346, No. 6208, P. 445-448.

28. D. Wegkamp, M. Herzog, Lede X., M.Gatti, P. Cudazzo, Christina L. McGahan, Robert E. Marvel, Richard F. Haglund Jr., A. Rubio, Martin. Wolf, J. Stähler. Instantaneous band gap collapse in photoexcited monoclinic VO_2 due to photocarrier doping. *Physical review letters*. 2014, Vol. 113, No. 21, P. 216401.

29. M. Liu, Harold Y. Hwang, H. Tao, Andrew C. Strikwerda, K. Fan, George R. Keiser, Aaron J. Sternbach, Kevin G. West, S. Kittiwatanakul, Jiwei Lu, Stuart A. Wolf, Fiorenzo G. Omenetto, X. Zhang, Keith A. Nelson, Richard D. Averitt. Terahertz-field-induced insulator-to-metal transition in vanadium dioxide metamaterial. *Nature*, 2012, Vol. 487, No. 7407, P. 345.

30. Kovneristy Yu.K., Lazareva I.Yu., Ravaev A.A. *Materialy, pogloshchayushchiye SVCH-izlucheniya* [Materials absorbing microwave radiation], Moscow, Nauka Publ., 1982, 164 pages. (In Russian).

31. Gorelov B.M., Konin K.P., Koval V.V., Ogenko V.M. A change in the microwave radiation reflection upon a dielectric–metal transition in Vanadium Dioxide. *Technical Physics Letters*, 2001, Vol. 27, No. 2, P. 157–159.

32. Beeson S., Dickens J., Neuber A. A high power microwave triggered RF opening switch. *Review of Scientific Instruments*. 2015, Vol. 86, No. 3, P. 034704.

33. F. Dumas-Bouchiat, C. Champeaux, and A. Catherinot. RF-microwave switches based on reversible semiconductor-metal transition of VO_2 thin films synthesized by pulsed-laser deposition. *Applied Physics Letters*. 2007, Vol. 91, No. 22, P. 223505.

34. J. Givernaud, A. Crunteanu, J.-C. Orlianges, A. Pothier, C. Champeaux, A. Catherinot, P. Blondy. Microwave power limiting devices based on the semiconductor–metal transition in vanadium–dioxide thin films. *IEEE Transactions on Microwave Theory and Techniques*. 2010, Vol. 58, No. 9, P. 2352-2361.

35. K.C. Pan, W. Wang, E. Shin, K. Freeman, G. Subramanyam. Vanadium oxide thin-film variable resistor-based RF switches. *IEEE Transactions on Electron Devices*. 2015, Vol. 62, No. 9, P. 2959-2965.

36. Jordan T. S., Scott S., Leonhardt D., Custer J. O., Rodenbeck C. T., Wolfley S., Nordquist C. D. Model and Characterization of VO_2 Thin-Film Switching Devices. *IEEE Transactions on Electron Devices*, 2014, Vol. 61, No. 3, P. 813-819.

37. M. J. Dicken, K. Aydin, I. M. Pryce, L. A. Sweatlock, E. M. Boyd, S. Walavalkar, J. Ma, and H. A. Atwater. Frequency tunable near-infrared metamaterials based on VO_2 phase transition. *Optics express*, 2009, Vol. 17, No. 20, P. 18330-18339.

38. T. Driscoll, S. Palit, M. M. Qazilbash, M. Brehm, F. Keilmann, B.-G. Chae, S.-J. Yun, H.-T. Kim, S. Y. Cho, N. M. Jokerst, D. R. Smith, D. N. Basov. Dynamic tuning of an infrared hybrid-metamaterial resonance using vanadium dioxide. *Applied Physics Letters*, 2008, Vol. 93, No. 2, P. 024101.

39. Appavoo K., Haglund Jr R. F. Detecting nanoscale size dependence in VO_2 phase transition using a split-ring resonator metamaterial. *Nano letters*, 2011, Vol. 11, No. 3, P. 1025-1031.

40. A. Crunteanu, G. Humbert, J. Leroy, L. Huitema, J.-C. Orlianges, A. Bessaudou. Tunable THz metamaterials based on phase-changed materials VO_2 triggered by thermal and electrical stimuli. *Terahertz, RF, Millimeter, and Submillimeter-Wave Technology and Applications X. – International Society for Optics and Photonics*, 2017, Vol. 10103, P. 101031H.

41. H. Liu, J. Lu, X.R. Wang. Metamaterials based on the phase transition of VO_2. *Nanotechnology*, 2017, Vol. 29, No. 2, P. 024002.

42. J. Leroy, G. Humbert, J.-C. Orlianges, C. Champeaux, P. Blondy, A. Crunteanu. Tunable Terahertz metamaterials based on hybrid integration of the VO_2 metal-insulator transition material. *Proc. of The 8th International Conference on Advanced Materials, ROCAM 2015*.

43. H. Kim, N. Charipar, E. Breckenfeld, A. Rosenberg, A. Piquéa. Active terahertz metamaterials based on the phase transition of VO_2 thin films. *Thin Solid Films*, 2015, Vol. 596, P. 45-50.

44. Shin J. H., Park K. H., Ryu H. C. Electrically controllable terahertz square-loop metamaterial based on VO_2 thin film. *Nanotechnology*, 2016, Vol. 27, No. 19, P. 195202.

45. G. Zhang, H. Ma, C. Lan, R. Gao, J. Zhou. Microwave Tunable Metamaterial Based on Semiconductor-to-Metal Phase Transition. *Scientific Reports*, 2017, Vol. 7, No. 1, P. 5773.

46. Zheng X., Xiao Z., Ling X. A tunable hybrid metamaterial reflective polarization converter based on vanadium oxide film. *Plasmonics*, 2018, Vol. 13, No. 1, P. 287-291.

47. X. Wen, Q. Zhang, J. Chai, L. M. Wong, Sh. Wang, and Q. Xiong. Near-infrared active metamaterials and their applications in tunable surface-enhanced Raman scattering. *Optics express*, 2014, Vol. 22, No. 3, P. 2989-2995.

48. Z. J. Thompson, A. Stickel, Y.-G. Jeong, S. Han, B. H. Son, M. J. Paul, B. Lee, A. Mousavian, G. Seo, H.-T. Kim, Y.-S. Lee, D.-S. Kim. Terahertz-triggered phase transition and hysteresis narrowing in a nanoantenna patterned vanadium dioxide film. *Nano letters*, 2015, Vol. 15, No. 9, P. 5893-5898.

49. Ch. Han, Edward P. J. Parrott, G. Humbert, A. Crunteanu, E. Pickwell-MacPherson. Broadband modulation of terahertz waves through electrically driven hybrid bowtie antenna-VO_2 devices. *Scientific reports*. 2017, Vol. 7, No. 1, P. 12725.

50. Y.-G. Jeong, J.-S. Kyoung, J.-W. Choi, S.-H. Han, H.-R. Park, N. Park B.-J. Kim, H.-T. Kim, H.-S. Kim, D.-S. Kim. Terahertz nano antenna enabled early transition in VO_2. *arXiv preprint* arXiv:1208.3269, 2012.

51. Sakai J. High-efficiency voltage oscillation in VO_2 planer-type junctions with infinite negative differential resistance. *Journal of Applied Physics*. 2008, Vol. 103, No. 10, P. 103708.

52. Lee Y. W., Kim B.-J., Lim J.-W., Yun S. J., Choi S., Chae B.-G., Kim G., and Kim H.-T. Metal-insulator transition-induced electrical oscillation in vanadium dioxide thin film. *Applied Physics Letters*, 2008, Vol. 92, No. 16, P. 162903.

53. Y. Zhao, J. H. Lee, Y. Zhu, M. Nazari, Ch. Chen, H. Wang, A. Bernussi, M. Holtz, and Zh. Fan. Structural, electrical, and terahertz transmission properties of VO_2 thin films grown on c-, r-, and m-plane sapphire substrates. *Journal of Applied Physics*. 2012, Vol. 111, No. 5, P. 053533.

54. Chen Z., Wen Q.-Y., Dong K. Ultrafast and broadband terahertz switching based on photo-induced phase transition in vanadium dioxide films. *Chin. Phys. Lett*., 2013, Vol. 30, P. 1–4.

55. T. L. Cocker, L. V. Titova, S. Fourmaux, H. -C. Bandulet, D. Brassard, J. -C. Kieffer, M. A. El Khakani, and F. A. Hegmann. Terahertz conductivity of the metal-insulator transition in a nanogranular VO_2 film. *Applied Physics Letters*. 2010, Vol. 97, No. 22, 221905.

56. J. S. Kyounga, S. B. Choib, H. S. Kima, B. J. Kimc, Y. H. Ahnd, H. T. Kimc, D. S. Kim. Nanoresonator Enabled Ultrafast All-optical Terahertz Switching Based on Vanadium Dioxide Thin Film. *AIP Conference Proceedings*, 2011, Vol. 1399, No. 1, P. 1027-1028.

57. Jeong Y., Bernien H., Kim D., et al. Electrical switching of terahertz radiation on vanadium dioxide thin film fabricated with nano antennas. *AIP Confer. Proc*., 2011, Vol. 1399, P. 967–968.

58. Y.-G. Jeong, H. Bernien, J.-S. Kyoung, H.-R. Park, H.-S. Kim, J.-W. Choi, B.-J. Kim, H.-T. Kim, K.J. Ahn, D.-S. Kim. Electrical control of terahertz nano antennas on VO_2 thin film. *Opt. Expr*., 2011, Vol. 19, No. 22, P. 21211 -21215.

59. M. Seo, J. Kyoung, H. Park, S. Koo, H. Kim, H. Bernien, B.J. Kim, J.H. Choe, Y.H. Ahn, H.-T. Kim, N. Park, Q.-H. Park, K. Ahn, D. Kim. Active Terahertz Nanoantennas Based on VO2 Phase Transition. *Nano Lett*., 2010, Vol. 10, P. 2064 – 2068.

60. Ch. Chen, Ya. Zhu, Y. Zhao, J. H. Lee, H. Wang, A. Bernussi, M. Holtz, and Zh. Fan. VO_2 multidomain heteroepitaxial growth and terahertz transmission modulation. *Applied Physics Letters*, 2010, Vol. 97, No. 21, P. 211905.

61. Q. Shi, W. Huang, J. Wu, Y. Zhang, Y. Xu, Y. Zhang, Sh. Qiao, and J. Yan. Terahertz transmission characteristics across the phase transition in VO_2 films deposited on Si, sapphire, and SiO_2 substrates. *Journal of Applied Physics*, 2012, Vol. 112, No. 3, P. 033523.

62. T.L. Cocker, L.V. Titova, S. Fourmaux, G. Holloway, H.-C. Bandulet, D. Brassard, J.-C. Kieffer, M.A. El Khakani, F. A. Hegmann. Phase diagram of the ultrafast photoinduced insulator-metal transition in vanadium dioxide. *Physical Review B*, 2012, Vol. 85, No. 15, P. 155120.

63.Y. Xu, W. Huang, Q. Shi, Y. Zhang, Y. Zhang, L. Song, Y. Zhang. Effects of porous nano-structure on the metal–insulator transition in VO2 films *Applied Surface Science*, 2012, Vol. 259, P. 256-260.

64. Zhan H., Astley V., Hvasta M. The metal-insulator transition in VO_2 studied using terahertz apertureless near-field microscopy. *Applied Physics Letters*. 2007, Vol. 91, No. 16, P. 162110.

65. Andreev V.N., Kapralova V.M., Klimov V.A. Effect of hydrogenation on the metal-semiconductor phase transition in vanadium dioxide thin films. *Physics of the Solid State*. 2007, Vol. 49, No. 12, P. 2318-2322.

66. S. A. Pauli, R. Herger, and P. R. Willmott. X-ray diffraction studies of the growth of vanadium dioxide nanoparticles. *Journal of Applied Physics*. 2007, Vol. 102, No. 7, P. 073527.

67. A. Cavalleri, Th. Dekorsy, H. H. W. Chong, J. C. Kieffer, and R. W. Schoenlein. Evidence for a structurally-driven insulator-to-metal transition in VO 2: A view from the ultrafast timescale. *Physical Review B*. 2004, Vol. 70, No. 16, P. 161102.

68. Chen C., Wang R., Shang L., Guo C. Gate-field-induced phase transitions in VO_2: monoclinic metal phase separation and switchable infrared reflections. *Applied Physics Letter*s. 2008, Vol. 93, No. 17, P. 171101.

69. Semenov A.L. Time of a semiconductor-metal phase transition induced by an ultrashort light pulse in vanadium dioxide. *Physics of the Solid State*, 2007, Vol. 49, No. 6, P. 1157-1160.

70. C. Chen, Y. Zhu, Y. Zhao, J.H. Lee, H. Wang, A. Bernussi, M. Holtz, Z. Fan. VO_2 multidomain heteroepitaxial growth and terahertz transmission modulation. *Appl. Phys. Lett*., 2019, Vol. 97, P. 211905.

71. Ch. Chen, Y. Zhu, Y. Zhao, J. H. Lee, H. Wang, A. Bernussi, M. Holtz, Zh. Fan. VO_2 multidomain heteroepitaxial growth and terahertz transmission modulation. *Applied Physics Letters*, 2010, Vol. 97, No. 21, P. 211905.

71. Balu R., Ashirt P.V. Near-zero IR transmission in the metal-insulator transition of VO_2 thin films. *Appl. Phys. Lett*., 2008, Vol. 92, P. 021904.

72. Ruzmetov D., Zawilski K.T., Narayanamurti V. Structure-functional property relationships in rf-sputtered vanadium dioxide thin films. *Journal of Applied Physics*, 2007, Vol. 102, No. 11, P. 113715.

73. I. Bychkov, D. Kuzmin, D. Kalenov, A. Kamantsev, V. Koledov, D. Kuchin, V. Shavrov. Electromagnetic waves generation in $Ni_{2.14}Mn_{0.81}GaFe_{0.05}$ Heusler alloy at structural phase transition. *Acta Physica Polonica A*, 2015, Vol. 127, No. 2, P. 588-590.

74. I.V. Bychkov, V.A. Golunov, D.S. Kalenov, A.P. Kamantsev, D.S. Kuchin, V.V. Koledov, D.A. Kuzmin, V.V. Meriacri, S.V. von Gratowski, M.P. Parkhomenko, A.V. Mashirov, V.G. Shavrov. The intrinsic radiation and electromagnetic wave reflection coefficient in the range of 8 mm of $Ni_{2,14}Mn_{0,81}GaFe_{0,05}$ and Ti-Ni alloys in the temperature interval near the phase transitions of the 1st and 2nd order. *Zhurnal Radioelektroniki - Journal of Radioelectronics*. 2014, No. 12, Available at http://jre.cplire.ru/jre/dec14/27/abstract_e.html

75. Sarafis P., Nassiopoulou A. G. Dielectric properties of porous silicon for use as a substrate for the on-chip integration of millimeter-wave devices in the frequency range 140 to 210 GHz. *Nanoscale research letters*, 2014, Vol. 9, No. 1, P. 418.

76. Peterseim T., Dressel M., Dietrich M., Polity A. Optical properties of VO_2 films at the phase transition: Influence of substrate and electronic correlations. *Journal of Applied Physics*, 2016, Vol. 120, No. 7, P. 075102.

77. V. R. Morrison, R. P. Chatelain, K. L. Tiwari, A. Hendaoui, A. Bruhács, M. Chaker, B. J. Siwick. A photoinduced metal-like phase of monoclinic VO_2 revealed by ultrafast electron diffraction. *Science*, 2014, Vol. 346, No. 6208, P. 445-448.

78. D. Wegkamp, M. Herzog, L. Xian, M. Gatti, P. Cudazzo, C. L. McGahan, R. E. Marvel, R. F. Haglund, Jr., A. Rubio, M. Wolf, J. Stähler. Instantaneous band gap collapse in photoexcited monoclinic VO_2 due to photocarrier doping. *Physical review letters*, 2014, Vol. 113, No. 21, P. 216401.

79. M. Liu, H. Y. Hwang, H. Tao, A. C. Strikwerda, K. Fan, G. R. Keiser, Aaron J. Sternbach, K. G. West, S. Kittiwatanakul, J. Lu, S. A. Wolf, F. G. Omenetto, X. Zhang, K. A. Nelson, R, D. Averitt. Terahertz-field-induced insulator-to-metal transition in vanadium dioxide metamaterial. *Nature*, 2012, Vol. 487, No. 7407, P. 345.

80. S. Kumar, F. Maury, N. Bahlawane. Electrical Switching in Semiconductor-Metal Self-Assembled VO_2 Disordered Metamaterial Coatings. *Scientific Reports*, 2016, Vol. 6, P. 37699.

81. H.W. Verleur, A.S. Barker Jr, C.N. Berglund. Optical properties of VO_2 between 0.25 and 5 eV. *Phys. Rev*., 1968, Vol. 172, No. 3, P. 788-798.

82. M. Currie, M.A. Mastro, V.D. Wheeler. Characterizing the tunable refractive index of vanadium dioxide. *Optical Materials Express*, 2017, Vol. 7, No. 5, P. 1697-1707.

83. C.F. Bohren, D.R. Huffman. Absorption and scattering of light by small particles. John-Wiley & Sons. 2008.

84. S.A. Maier. Plasmonics: Fundamentals and applications. Springer. 2007.

85. K.L. Kelly, E. Coronado, L.L. Zhao. The optical properties of metal nanoparticles: the influence of size, shape, and dielectric environment. *J. Phys. Chem. B*. 2003, Vol. 107, No. 3, P. 668-677.

86. R. H. Doremus. Optical properties of small silver particles. *J. Chem. Phys*. 1965, Vol. 42, No. 1, P. 414-417.

For citation:
V.V.Koledov, V.G.Shavrov, N.V.Shahmirzadi, T.Pakizeh, A.P.Kamantsev, D.S.Kalenov, M.P.Parkhomenko, S.V. von Gratowski, A.V.Irzhak, V.M.Serdyuk, J.A Titovitsky, A.A.Komlev, A.E Komlev, D.A.Kuzmin, I.V.Bychkov. The interaction of electromagnetic waves with VO_2 nanosized spheres and films in optical and extremely high frequency range. *Zhurnal Radioelektroniki - Journal of Radio Electronics*. 2018. No. 2. Available at http://jre.cplire.ru/jre/feb18/13/text.pdf.